Evolutionary conserved multifunctional nitric oxide synthesis proteins responding to bacterial MAMPs are located at the endoplasmic reticulum

Wenhui Zheng*[1], Hongchen Li*[1], Wenqin Fang*[1], Simon Ipcho[2], Rosanna C. Hennessy[2], Bjoern Oest Hansen[1,3], Guodong Lu[1], Zonghua Wang[1,4], Mari-Anne Newman[5], Stefan Olsson[1,6]#

***Co-first authors**

#Corresponding author

[1]State Key Laboratory for Ecological Pest Control of Fujian and Taiwan Crops, College of Plant Protection, Fujian Agriculture and Forestry University, Fuzhou, China.

[2]Section for Microbial Ecology and Biotechnology, Department of Plant and Environmental Sciences, University of Copenhagen, Frederiksberg C, Denmark

[3]OmicsDriven, Østergade 76, DK-4340 Tølløse, Denmark

[4]Institute of Oceanography, Minjiang University, Fuzhou, China

[5]Section for Transport Biology, Department of Plant and Environmental Sciences, University of Copenhagen, Frederiksberg C, Denmark

[6]Plant Immunity Center, Haixia Institute of Science and Technology, Fujian Agriculture and Forestry University, Fuzhou, China

Authors contributions divided per authors

WZ Deletion and complementation work on the heme reductase the NODs and the first Heme protein we deleted and phenotype analysis. Manuscript writing and correction

HL Deletion and complementation of Heme protein and phenotype analysis including of NO measurements for Confocal microscopy. Manuscript writing and correction

WF Complementation of the heme reductase gene with a mouse heme reductase and phenotype analysis including growth, conidiation and pathogenicity. Manuscript correction.

SI MAMPS stimulation and NO measurements including inhibitor analysis, methods development for carrying out these analyses and experiments and performed the transcriptomic experiments, Manuscript writing and correction.

RH NO measurements of effect of HemeR and NOD deletions. Manuscript correction.

BOH Preparation of transcriptomic data for co-regulation analysis. Manuscript correction.

GD Acquisition of financial support for final research. Manuscript correction.

ZW Acquisition of financial support for final research. Manuscript correction.

MAN Initial idea, discussions, and preparation of MAMPs for testing. Acquisition of financial support for initial research. Manuscript correction.

SO Initial idea. Acquisition of financial support for initial research. Hypotheses generation from data and from literature as well as from bioinformatics, co-regulation analysis, phylogenetic and structure analysis, overall responsible for driving the work forward and methods development. Suggesting confirmatory analyses and experiments for additional functions. Main responsible for manuscript writing and coordination of the manuscript writing and corrections.

Abstract

Most Eukaryotic organisms produce nitric oxide (NO); however, the mechanisms underpinning NO's biosynthesis are only known in animals. In animals, there seems to be a non-described additional system for producing NO in many cell types, including blood vessels where NO is essential for blood pressure control. NO is known to be a signalling molecule of the innate immunity system in plants and fungi although no NO generation has yet been described. In the plant pathogenic fungus *Fusarium graminearum,* we demonstrate an extra NO-producing system in fungi that seems also present in mammals and plants and, thus, likely the evolutionary original. The discovered NO-producing enzymes are already well-known sterol-producing enzymes with more than one function. Both these enzymes are targets for statins and the major fungicides; thus, the NO production of the new system has consequences for agriculture (pathogen resistance and control) and medicine (blood pressure control, immunity and sepsis).

Introduction

Organisms rely on NO as a signalling and effector molecule for numerous physiological and cellular processes. NO is a diffusible, short-lived [1], reactive free radical that acts as a secondary messenger [2,3] and NO production is a hallmark of the basal defence response against bacterial infections, also known as innate immunity. Plants and animals produce NO when they detect Microbial-Associated Molecular Patterns (MAMPs) [2,4,5]. MAMPs are conserved molecular patterns shed from microbes recognized and responded to by host organisms [6].

The NO production is mainly catalyzed by the enzyme Nitric Oxide Synthase (NOS), which converts L-arginine to citrulline and NO through the intermediate N-hydroxy-L-arginine (NOHA), as reviewed by [7]. The archetypal NOS consists of two parts; an N-terminal oxygenase containing the arginine binding site with heme and a tetrabiopterin domain, a central calmodulin (CaM), and the C-terminal reductase part contains FAD, FMN and an NADPH binding site. The enzyme is active in its homodimer form and is regulated by Ca^{2+} and CaM [7,8].

NOSs are thus proteins containing two main parts, a Cytochrome P450 (CYP) heme-binding part and an NADP Dependent Cytochrome P450 (NCP) reductase part. To become active, they dimerize aided by CaM and $Ca^{2+,}$ and the Heme-reductase part (the NCP) transports electrons to the heme in the heme-binding CYP in the paired proteins [8]. NO synthesis is initiated with heme-binding and activated by $O_{2,}$ and the reductase domain transfers NADPH-derived electrons to the oxygenase domain. NOSs are subjected to NO-self-regulation since NO binds to the iron in the heme and blocks NO synthesis at high NO concentrations [8,9]. NOSs are similar to cytochrome P450s, with the heme and reductase domains present in both enzymes [8].

In mammals, NO is generated by the very well-characterized mammalian three different isoforms of NOS [10]. Two are constitutively expressed in the brain (neuronal NOS, nNOS) and within the endothelial cells (eNOS) the latter involved in regulating the arteries' vasodilation. During microbial infection, the inducible NOS (iNOS) located within macrophages produces NO and mediates bacteria elimination [10]. In humans, the iNOS is part of a structural complex that contains the cationic amino acid transporter (CAT1), arginosuccinate synthetase (ASS), arginosuccinate lyase (ASL), the NOS and the heat shock protein 90 (HSP90). ASL and ASS are enzymes responsible for producing the substrate, arginine, fed directly to the NOSs. Disruption of the complex's structural integrity is detrimental to NO production [11].

Although shreds of evidence of NO-production have been reported in fungi and plants, their NOS orthologs have still not been found using sequence homology [12–14]. In Arabidopsis, a NOS-associated enzyme (AtNOA1) was discovered and found to contribute to the induction of a NO burst in response to the MAMP lipopolysaccharides (LPS) [15,4,16,17,3]. The AtNOA1 sequence did not resemble the archetypal NOS but was similar to a snail protein exhibiting NOS-like activity [15]. It was later found to be a cGTPase and not to have anything to do directly with NO production [18].

In fungi, genes encoding enzymes responsible for NO production from arginine, like NOSs, are unknown. While the *Aspergillus* species are reported to harbour genes with sequence homology to the mammalian NOS, functional analysis is lacking [8]. Previous studies have shown that yeast NOS-like proteins can be detected in filamentous fungi using antibodies; however, the sequence of the detected proteins has not yet been reported [19,20], nor are there any similarities between the NOS-sequences to the yeast genome sequence [13]. Nevertheless, NO has been shown to affect various stages of the fungal lifecycle ranging from germination to sporulation [14,21–23,13]

In addition to arginine, nitrite is a substrate for NO-formation in animals and plants, illustrating redundancies for this radical production [24–27]. The nitrate reduction pathway is involved in NO production in plants, it is, however, not alone responsible for NO production in plants [28]. The same was found when nitrate and nitrite reductase were deleted in the fungus *Magnaporthe oryzae*. The deletion mutants still produced NO and showed no altered phenotypes [14]. Nitrite and nitrate have also been proven to be a source of NO in *F. graminearum* triggered by host perception in the rhizosphere during the precontact phase using the model monocot *Brachyopodium distachyon*. These authors also concluded that nitrite/nitrate reductase only partially contributes to NO production in *F. graminearum* [29]. Results pointing to additional NO souces than nitrite/nitrate reduction was also found for NO formed by *Aspergillus nidulans* niaD. NO formation was not abolished in niaD deletion mutants but roughly halved, and nitrite and nitrate accumulated in ammonium media free from nitrate/nitrite, especially in the niaD deletion mutant [30], further indicating there should be another source of NO getting oxidized to nitrite and nitrate.

We had selected the model strain *Fusarium graminearum* strain PH1 (teleomorph *Gibberella zeae*) to investigate [31] whether fungi possess an immune system response to bacteria. The fungus is a severe pathogen of many kinds of grass, including wheat and causes Fusarium head blight (FHB), crown rot (FCR) and root rot (FRR) [32]. Simultaneously, it is a soil-borne fungus active in the plant rhizosphere [32], where it has to co-exist with many bacteria, neutral, beneficial and detrimental to the fungus [33]. We have previously shown that the transcriptome of *F. graminearum* responds specifically and rapidly to purified bacterial MAMPs by upregulating genes involved in Eukaryotic innate immunity responses [33]. Our former study served as a starting point to determine whether NO formation is part of a fungal innate immune response and if so identify the proteins responsible for synthesizing NO and if they could have similarities to known systems of NO formation.

Hypotheses: Our first hypothesis is that NO is produced in response to purified bacterial MAMPs as part of an innate immune response [33]. The second hypothesis is that NO is produced primarily from arginine, like normal NOSs, and not nitrite/nitrate through the nitrate reduction system. If the first and second hypotheses that NO is produced from arginine in response to bacterial MAMPs, NO might be produced by a non-conventional NOS system (hypothesis 3) where the heme protein and the heme-reductase belong to separate proteins that together produce NO since orthologues of mammalian type NOSes are not present in fungi or plants [14,28].

Results

NO production in response to bacterial MAMPs

NO is known to be elicited in response to bacterial MAMPS in plants and animals. We thus exposed the fungus to various MAMPs under the asme type of nongrowing conditions we had previously used for exposing fungal biomass to bacterial MAMPs [33]. The level of accumulated NO by the fluorescent NO probe dye (DAF-FM DA) was measured after 10 hours of elicitation. Similar to in mammals, full-length flagellin FFLG, but not the short FLG22 used to elicit NO responses in plants [34], was found to be the most consistent elicitor of NO in the fungus (**Fig. 1A**) and was used as a reference in the subsequent investigations even though the commercial flagellin preparation contained small non-declared amounts of sucrose [33]. We performed a control experiment under the same conditions to be sure that we detected gaseous NO developing as a response to the bacterial MAMP flagellin. For the control experiment, we used the Luminol-H_2O_2 fluorescence method [35]. With that, we developed a technique for head-space detection,

136 detecting the chemiluminescence in a scintillation vial with the reactants in an open Eppendorf tube insert
137 and the fungal biomass in water with or without flagellin added to the scintillation vial (See **Supplementary**
138 **file SF2** for the experimental setup and results). The NO donor NONOATE was used in a preceeding control
139 experiment instead of the fungus and flagellin to test whether the technique worked and whether the
140 amount of reactants in the Eppendorf tube were enough. Although very selective for NO, this technique
141 was not used further since the DAF-FM DA can be used in microtiter wells and analysed by a microplate
142 reader so that several measurements and replicates can simultaneously be run and that also can be used in
143 microscopy.

144

145 **Test if NO production is sensitive to standard NOS inhibitors**

146 In mammals, iNOS is regulated by signalling components such as phosphatidylinositol-3-kinases (PI3K),
147 Phosphatase and tensin homolog (PTEN), and Calcium influx and Calmodulin [36,37]. It is also well-
148 documented that NOSs use arginine as a substrate to generate NO [38]. A series of signalling inhibitors were
149 applied to query if similar characteristics governed the NO-producing enzyme in *F. graminearum* as in the
150 mammalian system. PI3K was inhibited with ZSTK474 and wortmannin, and PTEN was inhibited with
151 BpV(HOpic). Inhibition of both signalling components showed a decreased level of NO production (**Fig. 1A**).
152 Extra-cellular calcium and intracellular calmodulin were inhibited with EGTA and W7, respectively.
153 Chelation of calcium ions showed a moderately decreased NO response (**Fig. 1B**), whereas inhibition of
154 calmodulin completely inhibited NO production. The arginine analogue L-NNA, which an iNOS cannot
155 metabolize, was added to elicited cultures as a competitive inhibitor (**Fig. 1B**). The results showed that the
156 accumulation of NO signal was decreased compared to the control indicating that the NOS-system
157 response to bacterial MAMPs in *F. graminearum* uses arginine as substrate as mammalian NOSes and that
158 is also what seems to be the case for NO production during spore germination of the relatively closely
159 related fungus *Magnaporthe oryzae* [14].

160

161 **Bacterial MAMPs increase intracellular calcium levels**

162 When Ca^{2+} levels increase intracellularly, calmodulin is known to interact with and activate NOS [39,40,37,41]. To
163 test if calcium signalling is involved in the MAMPs detection, intracellular Ca^{2+} levels following bacterial
164 MAMPs challenges were investigated, and intracellular calcium increases above water controls using the
165 intracellular fluorescence calcium indicator Fluo4 AM that can be loaded into cells. Our results show
166 increasing green fluorescence indicating increasing intracellular Ca^{2+} concentration triggered by the
167 bacterial MAMPs treatments (**Fig. 1C**) that also triggered the NO responses (**Fig. 1A,B**).

168

169 **Standard substrates for NO production by NOSes are used for NO production**

170 The ability of *F. graminearum* to utilize exogenous chemicals as substrates were tested. Arginine, the
171 established substrate in mammalian systems, was added into bacterial MAMPs challenged cultures.
172 Interestingly, the NO production rate increased very fast due to arginine addition and then completely
173 stopped (**Fig. 2A**). To assess the possibility of NO production from nitrite (**Fig. 2B**), this was exogenously
174 injected into MAMPs challenged fungal cultures. Interestingly, in both experiments with exogenous
175 arginine and nitrite, the NO produced approximately doubled at 4h compared to at 2h. However, contrary
176 to the arginine experiment, NO accumulation continued post-spiking. To test if the effects were additive
177 exogenous nitrite and arginine were added in different sequential combinations. The results showed that
178 adding nitrite promoted a higher NO production rate when arginine was added later. A typical arrest of NO

179 production post arginine addition followed. When arginine was added before nitrite exogenously, a NO
180 burst was observed, followed by NO production's complete arrest. The addition of nitrites following the
181 arrest did not promote further NO production (**Fig. 2C and D**).

182 In conclusion, our results indicate that both arginine and nitrite can be substrates for the oxidative or
183 reductive formation of NO [14], but only the arginine additions result in rapid cumulative increases in the
184 DAF-FM fluorescence and indicate a high effective NO concentration since NO is very short-lived in cell
185 systems [1]. These results indicate that mainly arginine is responsible for a high transient concentrations of
186 NO that can be used for fast signalling. The rapid increases seemed to self-inhibit NO formation from
187 arginine as expected if it is formed by a heme protein similar to iNOS in mammals [8,9], supporting that
188 arginine is the primary substrate for quick NO formation in response to bacterial MAMPs.

189

190 **Finding candidate NO production genes in *F. graminearum***

191 Our experiments thus indicated that the NO-generating system in *F. graminearum* must be very similar to
192 the mammalian system [8]. Nevertheless, there are no classic NOS candidate genes in fungi [42]. The NOS-
193 domain PF02898.15 is usually used as a signature for finding nitric oxide synthetase enzymes [43]. Since no
194 usual NOS genes encoding a protein with a PF02898.15 domain is present in any predicted *F. graminearum*
195 proteins, there must be a different domain organization in the responsible protein protein or proteins. We
196 know from the literature that NOSes need to dimerize for NO to be produced, and this dimerization is Ca^{2+}-
197 dependent. It also means that electron transport goes from the heme-reductase domains in one protein to
198 the heme domain in the other [8]. Thus, there could be another way to bring together a NOS-like heme
199 domain-containing protein and NOS-like heme reductase containing all the other domains of a classic NOS.
200 The heme domain alone in a NOS has similarities to a **CY**tochrome **P**450 heme (**CYP**), and there are many
201 CYP-proteins in *F. graminearum*. We thus turned our interest to find a possible separate **N**ADPH-
202 **C**ytochrome **P**450 reductase (**NCP**) containing all the other domains necessary for a NOS-NCP involved in
203 NO-production [8].

204 The enzyme we are looking for is an ***F. g**raminearum* **NCP** involved in NO production, an **$FgNCP_{NO}$**. (from
205 now onwards, we write gene and protein abbreviations in bold where they are first introduced in the text
206 and the proposed cellular function as a subscript). We used the amino acid sequence of the C terminal
207 non-heme part of the Mouse iNOS (NP_035057.1) as bait and made a BLAST search against the *F.*
208 *graminearum* proteome. We only found 2 candidates $FgNCP_{NO}$ (FGSG_ FGSG_08413 and FGSG_09786),
209 with high similarity and containing all necessary domains [8] (**Supplementary File SF2**). Both genes contain
210 regions that indicate NADPH-dependent Cytochrome P450 heme reductases (NCPs) that could be involved
211 in transporting electrons from NADPH to a heme-containing protein that produces the NO from a reaction
212 between arginine and O_2.

213 We decided to use our previous transcriptome data to prioritize which gene to study in detail
214 (**Supplementary Data1**) to test if any of the two candidate genes are co-regulated with a putative *F.*
215 *graminearum* **N**itric **O**xide **D**ioxygenase (**FgNOD**) needed to protect a NO producing cell from NO [44]. We
216 calculated the correlation coefficients (Pearson) for transcription of the putative *$FgNCP_{NO}$* candidates of the
217 two putative *FgNODs* for all *F. graminearum* genes in 113 transcriptomes from data from our previous
218 experiments where *F. graminearum* has been exposed to different bacterial MAMPs (see methods) and
219 sorted the genes in order of highest to lowest correlation (**Supplementary File SF3**). We found that only
220 FGSG_09786 was highly correlated in expression with the two putative NODs, FgNOD1 and FgNOD2
221 (FGSG_00765 and FGSG_04458). Both NOD genes are similar to NO dioxygenases in *Candida albicans* that
222 are experimentally verified [45] and also to a NOD annotated for *Fusarium sporothrichiodes* (**Supplementary**

223 **File SF2**) FgNOD1 is almost identical to the *F. sporothricioides* protein (100% cover E-value 0 and identity
224 98%), and FgNOD2 is similar to FgNOD1 (90% cover, E value 2e-117 and identity 45.61%). FgNOD1 and
225 FgNOD2 have recently been confirmed to be responsive to nitrosative stress and have the suggested
226 functions in removing NO [46]. The correlation of expression of the two NODs and FGSG_09786 suggests that
227 FGSG_09786 is a putative $FgNCP_{NO}$ (**Fig. 3**). The other possible $FgNCP_{NO}$ gene, FGSG_08413, was not highly
228 expressed in our bacterial MAMPs data and even showed a slight negative correlation with the two
229 putative FgNODs (**Fig. 3**). It is thus not likely encoding a $FgNCP_{NO}$. FgNOD1 is also more closely co-regulated
230 with $FgNCP_{NO,}$ suggesting that FgNOD1 is the primary NOD responsible for limiting NO stress, assuming
231 $FgNCP_{NO}$ directly participates in NO-generating activities.

232 **Deletions of putative $FgNCP_{NO}$, *FgNOD1* and *FgNOD2* and the response to bacterial MAMPs**

233 **NO production of mutants:** Deletion and GFP complementation strains for $FgNCP_{NO}$, *FgNOD1* and *FgNOD*2
234 were constructed (see methods (**Fig. S1**)) and tested for NO production. We found that the $\Delta FgNCP_{NO}$ had
235 a radically lower accumulation rate of DAF-FM fluorescence than the WT, indicating a reduced NO
236 production rate (**Fig. 4A**). When focusing on the difference between controls and induced responses using
237 bacterial free washings from washed bacteria (see methods), the NO response to the MAMPs was
238 markedly diminished (**Fig. 4B**). Of the two NOD deletions, only *ΔFgNOD1* showed a tendency to respond to
239 NO-signals faster than WT suggesting that FgNOD1 could be the main counterpart to the NO generating
240 system limiting NO stresses in *F. graminearum*.

241 **Subcellular localization of $FgNCP_{NO}$, FgNOD1 and FgNOD2 and NO production:** $FgNCP_{NO}$-GFP localizes to
242 endoplasmic reticulum (ER)-like structures in spores and hyphae (**Fig. S2 I**) and could also be shown to co-
243 localize with an ER-tracker (**Fig. 5A**), and an mCherry labelled ER-marker protein (**Fig. 5B)**. In contrast,
244 FgNOD1-GFP localizes to mainly to the cytoplasm in germinating conidia, and FgNOD2-GFP localizes to
245 cytoplasm and dots (**Fig S2 II and III**). Since the $FgNCP_{NO}$-GFP localizes to ER, we tested if NO production
246 also occurs preferentially in the ER to check further the likelihood that it is involved in NO production. DAF-
247 FM is a non-fluorescent fluorescein derivative that only becomes strongly fluorescent after reacting with
248 NO. DAF-FM is loaded in the diacetate form, DAF-FM DA, in the same way as FDA. The two acetate groups
249 are cleaved off by always-present cytosolic esterases leaving strongly fluorescent and relatively hydrophilic
250 fluorescein, accumulating in the cytosol if the plasma membrane is intact. However, the membranes are
251 slightly permeable to fluorescein; thus, the external medium and intracellular compartments, like vacuoles,
252 will be coloured within minutes. Consequently, we needed to load the fungus with DAF-FM DA as fast as
253 possible and see where the first green signal appeared after it had been taken up and reacted with NO. We
254 did not need to use MAMPs to elicit NO as the background NO formation rate was nearly too fast to get
255 good images without green signals leaking out from the fungus. Good signals appeared already minutes
256 after the addition of the NO probe. As can be seen, NO is produced in the ER but also in non-ER dots (**Fig.
257 5C**).

258 We can thus conclude that the heme reductase $FgNCP_{NO}$ is involved in NO production, and the NO
259 production occurs in the ER where the heme reductase is located and as wella as in dots that might be
260 peroxisomes where NO_2 and NO_3 reduction is known to take place. FgNOD1 is likely the FgNOD that could
261 be the main responsible for limiting NO in the nucleus and cytoplasm, and FgNOD2 might be active in the
262 dots (that are maybe peroxisomes) (**Fig S2 II and III**). Our transcriptome data thus indicated that FgNOD1 is
263 the primary NOD since it is most co-regulated with $FgNCP_{NO}$ (**Fig. 3**).

264

265 **Phenotypic effects of deletion of NO generating and NO protecting proteins**

266 Phenotype analysis showed that deletion of the $FgNCP_{NO}$ had little effect on growth rate (**Fig. 6A and Fig.**
267 **S3A**), but conidia formation was inhibited (**Fig. 6B**), and there was no formation of sexual spores (**Fig. S3B**).
268 Pathogenicity was also reduced in the $FgNCP_{NO}$ (**Fig. 6C** and **Fig. S4**. That is probably mainly caused by the
269 lack of production of the phytotoxic metabolite deoxynivalenol (DON) (**Fig. 6D**) since the trichothecene
270 DON is needed for full pathogenicity [47]. NO signalling is known to be involved in conidial production[30], so
271 the lowered conidia production could result from this lack of NO (**Fig. 6B**). There was otherwise minor or
272 no effect of the *$FgNCP_{NO}$* mutation on stress phenotypes indicating cell wall and membrane changes,
273 except the *$\Delta FgNCP_{NO}$* mutant was somewhat more sensitive to Na^+ and K^+ ionic stresses (data not shown).
274 The *NOD* deletions had minimal effect on growth and infection phenotypes, indicating that NO protection
275 is not very important for pathogenicity or growth on traditional sterile lab media (**Fig. 6**).

276

277 **Finding a putative heme protein that works together with $FgNCP_{NO}$ to produce NO**

278 Since we found the NO-producing heme-reductase ($FgNCP_{NO}$) and knew where it is located, we turned our
279 interest towards the heme protein that should be the one making the NO using electrons delivered from
280 the $FgNCP_{NO}$. The expected heme-binding protein should have the following characteristics except
281 predicted heme binding. 1. It should be co-regulated with the $FgNCP_{NO}$ in transcriptome data when the
282 fungus is exposed to bacterial MAMPs. 2. It should be predicted to be located at the ER membrane.

283 One heme protein was on top of our list for genes co-regulated with $FgNCP_{NO}$ when exposed to bacterial
284 MAMPs, FGSG_07925 (**Supplementary File SF5**). The only problem was that it was not predicted to be
285 localized to the ER but so was not $FgNCP_{NO}$ either iosing PSORTII. We knocked out FGSG_07925 and
286 complemented it with FGSG_07925::GFP, but this protein did not localize to the ER (**Fig. S6**). Neither did
287 the mutant show any notable phenotype except a decrease in conidiation (**Fig. S7**).

288 We later found that the localization prediction server DeepLoc 1.0 [48] correctly localized $FgNCP_{NO}$ to ER, as
289 we had found experimentally. Using DeepLoc and our transcriptomic data from the MAMPs experiments
290 we found that only *FGSG_01000* was predicted to encode an ER-localized heme-containing protein that is
291 also co-expressed with $FgNCP_{NO,}$ and that expression is in a close to 1/1 ratio of max expression compared
292 to the max expression of $FgNCP_{NO}$ (**Table S8 and Supplementary File SF6**) making it a better candidate for
293 an ***F. g**raminearum* **CY**tochrome **P**450 involved in **NO** production, a **$FgCYP_{NO}$**

294 In this case, we could obviously not trust PSORTII for localization prediction since it wrongly predicts the
295 localization of the ER-localized $FgNCP_{NO}$. (**Table S5**).

296

297 **Deletion of the putative $FgCYP_{NO}$: Localization, NO production rate and effect on phenotype**

298 We decided to knock out *$FgCYP_{NO}$* (FGSG_01000) and test for NO-production. We successfully knocked it
299 out (**Fig S9)** and could show a significantly decreased NO production for *$\Delta FgCYP_{NO}$* to the same level as for
300 the *$\Delta FgNCP_{NO}$* (**Fig. 7A**) using our newly developed technique employing confocal microscopy to get
301 cleaner data and avoid fluorescent specks not related to the NO-production (See methods). As predicted,
302 the $FgCYP_{NO}$ localizes to ER-like structures (**Fig.7 B**). We can conclude that the putative $FgCYP_{NO}$ is ER
303 located and responsible for NO production.

304 Phenotype analysis of the *$\Delta FgCYP_{NO}$* showed some effect on growth (**Fig. 8A**) but more effect on stress
305 tolerance (**Fig. 8B and Fig. S10A**) and pathogenicity (**Fig. S10 B and C**) and a decrease in DON production
306 (**Fig. 8C)**. Although a notable decrease in DON production was registered, DON production was not absent,
307 as for the *$\Delta FgNCP_{NO}$*. The stress phenotypes indicate also that **$FgCYP_{NO}$** plays a role in the cell wall and

plasma membrane integrity. We knew that sexual spore formation was reduced in the Δ*FgNCP$_{NO}$* (**Fig. S3B),** so we decided to also look at the effects of ascospore formation for both mutants. Both Δ*FgNCP$_{NO}$* and *ΔFgCYP$_{NO}$* formed abnormal asci, even if the latter formed similar amounts of perithecia as the WT (**Fig. S13**).

Phylogenetic analysis of the two proteins involved in NO production

Phylogenetic analysis showed a high degree of conservation of both the NCP$_{NO}$ and the CYP$_{NO}$ in a wide range of Eukaryotes (**Fig. 9**). Most of the putative CYP$_{NO}$-proteins were, to our surprise, annotated as CYP51 (ERG11 yeast) involved in sterol synthesis. In contrast, the NCP$_{NO}$-proteins were annotated as NADP-dependent cytochrome P450 protein reductases as expected (**Supplementary File SF2 and SF6**). The domain organization for all these othrologous proteins was almost identical to the mouse iNOS but separated into two proteins with a predicted N-terminal hydrophobic attachment to the ER membrane (**Fig. 10 and Supplementary File SF7 and SF8)**. The FgCYP$_{NO}$ contain a CaM-binding domain that could indicate its activity is positively regulated by calcium, as our result indicates (**Fig. 2 and 3**). FgNCP$_{NO}$ is involved in DON production necessary for full plant pathogenicity, and this production might also be Ca-regulated, as shown in the literature [49]. We find that the FgNCP$_{NO}$ orthologues contain a signal for a putative CaM-binding region using the CaMELS web tool [50], possibly explaining why DON-toxin production [49] and pathogenicity are dependent on Ca.

Can FgCYP$_{NO}$ also be involved in ergosterol biosynthesis?

The FgCYP$_{NO}$ is well conserved in fungi but mainly annotated as a cytochrome P450 (CYP51) having a role in sterol synthesis, converting lanosterol to the next step in the sterols synthesis on the way to ergosterol in fungi and cholesterol in animals and other sterols in other eukaryotes [51]. The final products, ergosterol or cholesterol, are necessary for endocytosis. Lack of the final product ergosterol in the membrane and accumulating lanosterol should inhibit endocytosis previously as shown in the literature [52]. Thus, if the FgCYP$_{NO}$ is also involved in ergosterol synthesis, endocytosis should be decreased in the *ΔFgCYP$_{NO}$* strain [53]. Indeed, endocytosis was shut off as the standard endocytosis probe FM4-64 was not taken up and quickly internalized (**Fig. 11A**) in the *ΔFgCYP$_{NO}$* strain, indicating that the deleted heme protein (FgCYP$_{NO}$) is likely involved in sterol production as many of its orthologues are, and it is consequently an **FgCYP$_{NO,ERG}$** with at least these two functions.

Regulation of the genes involved in ergosterol, NO and DON production during infection in published transcriptomes from *in planta* experiments

We have previously downloaded publicly available transcriptomic *in planta* data from plant infection experiments with *F. graminearum* as a pathogen [54]. The first dataset from a time course of infection is interesting since the deletion of FgNCP$_{NO}$ completely stopped DON production (**Fig. 6D**). From the literature, it is known that the *FGSG_03535* gene in the co-regulated trichothecene gene cluster making DON (the TRI cluster) is a P450 heme protein named TRI4 [55]. It also localizes to the ER [56], could named as a FgCYP$_{TRI}$ since it is a CYP necessary for making a reduction step in the DON synthesis. If FgNCP$_{NO}$ is also a reductase delivering electrons to the FgCYP$_{TRI}$ protein, it should be co-regulated with FgCYP$_{TRI}$ in the *in-planta* data and upregulated during different phases of infection (Hours Post Infection, HPI). In plant infection transcriptome dataset, the FgCYP$_{TRI}$ is strongly co-regulated with the FgNCP$_{NO}$ during infection, and FgCYP$_{TRI}$ is upregulated after 24HPI. However, the NO-producing FgCYP$_{NO}$ is not co-regulated with

350 $FgNCP_{NO}$ during infection (**Fig. 11B**), indicating that $FgNCP_{NO}$ should be named **$FgNCP_{NO,TRI}$** since it is involved
351 in reducing heme proteins needed for both NO formation as well as DON synthesis.

352 Sterol formation is essential and there are only two NCPs with the correct structure (FGSG_09786 and
353 FGSG_08413) (**Fig. 3**), and we could not find any or a minimal effect on endocytosis when deleting
354 $FgNCP_{NO,TRI}$ (**Fig. 11A**), the other heme reductase (FGSG_08413) could be involved in ergosterol production,
355 also delivering electrons to $FgCYP_{NO,ERG}$. Consequently, both heme reductases should be able to
356 complement each other for ergosterol synthesis. Therefore, the remaining heme reductase (FGSG_08413)
357 could have a function as a reductase not involved in DON or NO production but only in ergosterol
358 production, a **$FgNCP_{ERG}$,** and the $FgNCP_{NO,TRI}$ would then be a reductase involved in ergosterol production as
359 well, a **$FgNCP_{NO,TRI,ERG}$**. If this is the case, and since there is probably not any increased NO formed during
360 the first 144HPI indicated by the absence of upregulation of the $FgCYP_{NO,ERG}$, FgNOD1 and FgNOD2 (**Fig.**
361 **11C**), there should be an inverse relationship between $FgNCP_{NO,TRI,ERG}$ and $FgNCP_{ERG}$ expression during
362 infection since ergosterol synthesis is necessary under aerobic conditions [53] and the $FgNCP_{NO,TRI,ERG}$ get
363 increasingly occupied with the $FgCYP_{TRI}$ for producing DON. This inverse relationship is indeed the case (**Fig.**
364 **11D-E**), suggesting that both proteins are involved in ergosterol synthesis providing $FgCYP_{NO,ERG}$ with
365 electrons.

366 A way to directly test this conclusion is to investigate *$FgCYP_{NO,ERG}$* and *$FgNCP_{NO,TRI,ERG}$* expression in WT (PH1)
367 and compare it with the expression of the same genes in the *$\Delta FgNCP_{NO,TRI,ERG}$* strain that does not make
368 DON but is capable of limited endocytosis (**Fig. 11A**) that needs ergosterol to work. We made this
369 comparison using RT-qPCR and can show that $FgCYP_{NO,ERG}$ is strongly and significantly upregulated, and
370 $FgNCP_{ERG}$ is slightly, but not significantly upregulated in the *$\Delta FgNCP_{NO,TRI,ERG}$* compared to the WT(PH1),
371 indicating that these genes are compensatory regulated in the mutant (**Fig. 11F**) explaining why the
372 *$\Delta FgNCP_{NO,TRI,ERG}$* still show some endocytosis (**Fig. 11A**).

373 **$FgNCP_{NO,TRI,ERG}$ can be complemented by an orthologues NCP from mouse**

374 The $FgNCP_{NO,TRI,ERG}$ protein is similarly organized in *F. graminearum* and mammals (**Fig. 10**) but annotated
375 as involved in the sterol synthesis, we complemented the *$FgNCP_{NO,TRI,ERG}$* with the heterologous gene from
376 mouse (NM_008898). The mouse gene localized to ER as predicted and restored colony growth rate, but
377 not conidia formation or the trichothecene mycotoxin DON's production. However, the trichothecene-
378 dependent pathogenicity on wheat coleoptiles was restored, possibly indicating that another *Fusarium*
379 *graminearum* species complex trichothecene than DON [57] could have become the main product when
380 electrons were delivered from the MouseNCP to the CYP_{TRI} (TRI4 gene) (**Supplementary Fig. S11**). Most
381 importantly, the MouseNCP could restore the NO production (**Fig.12**), indicating that in mammals, the CYP
382 and NCP involved in converting lanosterol in the cholesterol synthesis pathway should be able to produce
383 NO also in mice.

384 **Interactions between the $FgCYP_{NO,ERG}$ and $FgNCP_{ERG}$**

385 Both proteins localize to the cytosolic side of ER according to our results and the literature for orthologous
386 proteins in other organisms. At the ER they should interact to form NO or the ergosterol intermediate. We
387 used the yeast 2 hybrid technique (Y2H) to express the proteins in yeast without their N-terminal
388 membrane anchor and introns to detect eventual protein interactions but could not detect any physical
389 interaction (data not shown). We then tried bimolecular fluorescence complementation (BiFC) since that
390 can be used to detect if the proteins are close in vivo in *F. graminearum* but found no positive interaction
391 (data not shown). For both techniques a negative result is no evidence for no interaction. We have thus
392 not been able to confirm that these proteins interact closely and long enough to be recorded as positive
393 with any of these techniques. As an electron transport is needed for the essential sterol synthesis, we must

assume that they interact in some way, maybe for short times and at relatively long distances. According to the literature direct contact is not needed for efficient electron transport; on the contrary, that could even be counterproductive [58,59] (further discussed in the discussion below).

Discussion

Similarities and differences to NOS in mammals

There are apparent similarities between the ER-located NO-generating and lanosterol-reducing (**Fig. 9 and 10**) proteins and mammalian NOS. Calcium-dependent dimerisation is needed for NOS to be activated, at least for nNOS and eNOS [8]. As we have demonstrated, NO production in *F. graminearum* is stimulated by MAMPs. This stimulation leads to increases in the concentration of cytosolic Ca^{2+}.

The ER-located proteins involved in NO production in *F. graminearum* are predicted to be CaM-interacting (**Fig. 10**) and Ca^{2+} increases intracellularly induced by bacterial MAMPs (**Fig. 1C**) that triggers NO production (**Fig. 1A-B,2)**. CaM changes in conformation most likely help bring the two NO generating proteins closer together on the ER membrane, activating NO production (**Fig. 13A**). The ER-located $CYP_{NO,ERG}$ and $NCP_{NO,\ ERG,TRI}$ reducing system is remarkably conserved from Protista to Mammals (**Fig. 9-10**).

Electron transfer proteins where electrons are transferred between domains in the same proteins seem to be made efficient by quantum tunnelling electrons between precisely spaced domains [58,59]. Quantum tunnelling imposes severe constraints on essential proteins' evolution and can explain the high conservation of the involved proteins. This need for conservation can also explain why there are double and triple functions for the involved proteins with different roles in combinations with different proteins. Functionally conserved NCPs producing NO is supported by our successful complementation of the *F. graminearum* gene by the mouse's orthologue (**Fig. 12**).

Previously, in the literature it has been pointed out that the three classical NOS systems are not present quantitatively enough to generate NO in human vascular tissues, pointing towards additional NO generating systems also present in the microvasculature [60] and a p450 CYP is a good candidate for an additional system [61–64]. The conserved CYP-NCP pair that are responsible for sterol synthesis is a good candidate for such a system, since the mouse NCP could successfully complement the fungal NCP for NO production. Electron tunnelling between from NCPs to the CYPs at the ER membrane could also explain the flexibility in the CYPs ($FgCYP_{NO,ERG}$, $FgCYP_{ERG}$, $FgCYP_{TRI}$) and NCP ($FgNCP_{NO,TRI,ERG}$, $FgNCP_{ERG}$) used since there is no need for physical contact for electron transfer since electrons can tunnel between separate protein domains [58,59] even over as long distances as 100 nm in the case of heme proteins [65]. Long distance might not even be energetically problematic. Rather the opposite as close contact is less efficient for tunnelling [66]. If physical protein-protein contact is not needed the relative concentration of the involved proteins at the ER membrane will decide what is produced and how much,. What is mainly needed is changes in transcription and translation of the different proteins and that can be changed quickly.

Electron transfer between proteins attached to a membrane without needing physical contact offers an elegant and quick mode for changing product output while always keeping necessary sterol synthesis going. Since all proteins are membrane-attached and their orientation should be strongly affected by the membrane potential, the protein approaches are more likely to be productive since the proteins will be correctly oriented in a way that can result in an electron transfer. In combination with calcium binding to the predicted calmodulin sites (Fig. 10), the proteins' shape can also be changed further to even better promote electron transfer.

436

437 **Plant pathogenicity and NO generation**

438 It has recently been shown that NO is formed in *F. graminearum* as a response to-plant molecules' during
439 pre-plant contacts in the rhizosphere bot not inside the plant. A plant-sensing receptor triggers
440 downstream responses resulting in fungal NO-formation, and further downstream NO responses have
441 been identified [29]. Our results (**Fig. 10**) indicate that fungal $FgCYP_{NO,ERG}$ needed for NO production appear to
442 decrease when *in planta,* which would meet the challenge of not producing NO inside a plant since that
443 can activate plant defences [14,29]. Instead, *in planta,* the electron transfer from the $FgNCP_{NO,TRI,ERG}$ takes part
444 in DON production partly using the NO-generating enzymes (see above). The $FgNCP_{NO,TRI,ERG}$ has also been
445 well described enzymatically under its UniProt entry name I1RZE7_GIBZE as a protein having all the
446 necessary activities to take part in both DON and ergosterol synthesis [67]. DON is an inhibitor of translation
447 [68], and the innate immune responses in Eukaryotes depend on the quick upregulation of defence proteins
448 [69]. A shift from NO to DON production *in planta* (**Fig. 11B**) to attenuate the eventually turned-on plant
449 defences could be an evolutionary adaptation of *F. graminearum*. In native North American grasses, *F.*
450 *graminearum* seems to have evolved to colonize as an endophyte, disease with accompanying high DON
451 production is not triggered [70]. Production of large amounts of NO in planta would trigger the plant SA
452 defences and recruit plant PR proteins, as would exposure of ergosterol to the plant. Limiting plant access
453 to ergosterol, a known fungal MAMP, that plants react to should also avoid trigging plant defences [71,72].
454 The changing roles of the proteins *in planta* could might indicate an evolutionary adaptation to an
455 endophytic lifestyle, where plant defences stressing the fungus and counteracting DON responses from the
456 fungus balance the interaction with the plant allowing the fungus to grow inside the plant without plant
457 disease development. The higher levels of DON production produced in wheat and other Eurasian grasses
458 might be caused by the fungus being mistaken for a pathogen by these grasses, making the fungus a *de*
459 *facto* pathogen [70] responding with necrotrophic pathogenicity to the stresses imposed by the plant's
460 pathogen defence system..

461

462 **NO generation and essential sterol synthesis are intimately linked, and the system seems present in all**
463 **eukaryotes**

464 Our results unexpectedly revealed that NO generation and ergosterol synthesis are intimately connected.
465 The genes we found that are responsible for nitric oxide generation have been well characterized as part of
466 sterol synthesis. Sterol synthesis has even been well characterized previously in *F. graminearum* [73]. There
467 are 3 FgERG11/CYP51 genes responsible for critical sterol synthesis. The primary gene involved
468 (FGSG_01000, CYP51B) is the one we now find is responsible for NO production. For other organisms
469 (fungi, plants and animals), the genes catalysing this step in sterol synthesis are necessary under aerobic
470 conditions [53] and the human gene HsCYP51A can replace the ScER11 counterpart [74]. In *F. graminearum*,
471 that step is catalyzed by 3 paralogues [73], where 2 of the proteins complement each other's function for
472 ergosterol synthesis, as we also found (**Fig. 11**). The orthologous mouse NCP can replace $FgNCP_{NO,TRI,ERG}$
473 suggesting that both mammalian genes (**Fig 12**, **Supplementary Fig. S11)** needed for that specific step in
474 ergosterol synthesis are also involved in nitric oxide production as they are in *F. graminearum*.

475 Thus, it was sheer luck that we chose to investigate fungal NO production in *F. graminearum* since it has
476 many paralogues of this essential gene and that these can stand in for each other regarding essential sterol
477 synthesis, [73]. Genes encoding proteins catalysing the same chemical reaction have been assigned different
478 names in different organisms, although they have similar chemical functions. **Table 1** illustrates these
479 names compared to the names used in this paper. Finally, FGSG_08786, the $FgNCP_{NO,TRI,ERG}$ has been

480 chemically characterized and called FgCPR and suggested to take part in DON-synthesis or ergosterol
481 synthesis [67] as we also can confirm (**Fig. 6B**).

482 **Endocytosis and NO possible consequences**

483 Heme interaction with O_2 in the oxidative formation of NO from arginine is inhibited at high NO
484 concentrations since NO binds heme better than O_2 and blocks further NO production [9]. Thus iNOSes are
485 known to be self-inhibited [8,9]. Since the heme in the $FgCYP_{NO,ERG}$ is also used for reducing lanosterol in the
486 ergosterols synthesis, NO should also halt ergosterol synthesis [75] at lanosterol, inhibiting endocytosis
487 [52,76,77]. Interestingly, a complete stop in endocytosis was previously observed by us in *Rhizoctonia solani*
488 hyphae confronted with a bacterial biological control strain of *Burkholderia vietnamiensis* [78–80] while nitric
489 oxide was produced [78]. Those observations of NO formation inspired this study, together with the study on
490 fungal innate immunity [81] in *F. graminearum* but it is first now with this work we understand why
491 endocytosis became blocked.

492 A shutting down of endocytosis due to high NO concentration interacting with heme triggered by bacterial
493 challenges is likely an ancient system protecting primitive eukaryotes from pathogenic bacteria utilizing the
494 endocytosis mechanism to gain entry into the interior of the cells [82]. This general effect
495 infection/inflammation has on endocytosis should have broader consequences since, for example, LDL is
496 taken up by endocytosis [83] and depends on CYP51 function [84]. Since the heme-containing CYP51
497 (homologue to $FgCYP_{NO,ERG}$) is likely self-inhibited by NO formed during inflammation in the same way as
498 iNOSES this might explain inflammation-induced decreased LDL uptake and resulting health problems
499 linked to chronic inflammation [83].

500 **NO and ergosterol as antioxidants**

501 Both NO and membrane sterols are antioxidants that protect unsaturated membrane lipids from a
502 runaway chain reaction of lipid peroxidation with the formation of lipid peroxide radicals, lipox [85,86]. NO
503 and membrane sterols might be the original antioxidants protecting membranes in early eukaryotic
504 evolution when oxygen levels were low and the early eucaryotes were anaerobic. That could explain why
505 they are intimately connected in their synthesis and appear to be present in basically all Eukaryotes. Lipid
506 peroxidation is a severe problem for all aerobic life since life originated anaerobically and has never fully
507 adapted to high oxygen levels. Different protective measures have evolved, but a fundamental redesign of
508 the membrane components has not evolved outside bacteria. Eukaryotes use unsaturated membrane
509 lipids sensitive to oxidation to achieve necessary membrane fluidity. Some bacteria can instead produce
510 branched saturated fatty and use them in for the same purpose [87], offering better protection against
511 oxidation.

512

513 **Nitrogen limitations and NO production, possible consequences**

514 Fungi are generally nitrogen limited in nature. It also applies to *F. graminearum,* which is nitrogen and
515 sometimes carbon-limited inside the plant and dependent on autophagy for mobilizing carbon and
516 nitrogen from stores [88]. During the N-limited conditions both fungi and plants generally live under, they
517 should have evolved mechanisms to save nitrogen. The NOS formation of NO from arginine is less
518 problematic if the NO_2 or even NO_3 formed in that process could also be used to generate NO while making
519 NH_4^- through assimilatory reductions so that arginine can be replenished. However, our result with the
520 spiking experiments show that the effective concentrations of NO should be higher after spiking with
521 arginine since the rate of the increase indicates the effective NO concentration (**Fig. 2C**). This could mean
522 that the NOS-like arginine oxidation is the primary source of NO and the reductive pathway through nitrite

523 reductase is a secondary system needed for prolonged NO production and recycling of N. Thus assimilatory
524 nitrite/nitrate reduction in both plants and fungi could have evolved mainly as a mechanism to save N and
525 recharge the cells with arginine since a large amount of arginine is needed to make NO when challenged by
526 bacteria [89]. That could also explain why assimilatory nitrate/nitrite reduction is under the control of the
527 GATA factor AreA in fungi that regulates genes needed to use secondary nitrogen sources also regulates
528 secondary metabolite production since those metabolites are needed to interact with other organisms [90].

529 **Conclusion and overall conceptual model for what happens at the ER**

530 Our results show that the evolutionary ancient and very conserved sterol synthesis system in Eukaryotic
531 cells is involved in NO production. In *F. graminearum,* part of the system has a role in producing the
532 mycotoxin deoxynivalenol (DON) that inhibits translation [68] in the plant host cell and should lower plant
533 immune responses. *In vitro,* the fungus makes ergosterol and, but if severely challenged with bacteria NO
534 forms, likely stopping ergosterol synthesis at lanosterol, shutting down endocytosis and preparing the
535 fungus for bacterial defences. If attacked by plant defences *in planta,* the part of the system shift again but
536 to the production of DON to inhibit plant translation to attenuate plant defences (**Fig. 13B**) [68]. Our result
537 further imply that the cholesterol synthesis system in mammals also generates NO when receiving
538 inflammation signals which should have negative effects on LDL uptake and metabolism as well as
539 increased blood pressure linked to chronic inflammation [83].

540 Materials and Methods

541 **Maintenance and growth of *Fusarium graminearum* for plate-reader assays**

542 The wild type strain of *Gibberella zeae* ((Schwein) Petch) (anamorph *Fusarium graminearum* (Schwabe)
543 PH1 (NRRL31084) was originally obtained from the Agricultural Research Service Culture Collection,
544 National Center for Agricultural Utilization Research, Peoria, IL, USA. The wild-type and mutant strains
545 were stored as spores in 10% glycerol at -70°C. Cultures were maintained on minimal Defined Fusarium
546 Medium (DFM) at 21°C, in the dark and shaking at 150 rpm if necessary. The strains were cultured in YPG
547 liquid medium to get fungal biomass for DNA extraction [91]. Spore production was induced by fungal growth
548 in liquid RA medium (succinic acid, 50 g L-1; sodium nitrate, 12.1 g L-1; glucose, 1 g L-1 and 20 mL L-1 50X
549 Vogel's salts without nitrogen or carbon source) for 3 days. The spore suspension was filtered through
550 Miracloth, washed, and centrifuged twice at 5000 x g for 15 min.

551

552 **NO elicitation from *F. graminearum* using purified MAMPs in a plate reader**

553 NO production was measured using a 96 well plate assay with various potential elicitors, including MAMPs.
554 In each well, 2000 spores were cultured overnight in 100 µl of DFM (diluted 1:50) at 21°C in an incubator
555 without light. The growth medium was removed from the overnight culture to produce a thin mycelial mat
556 (network) attached to the bottom of the wells , and sterile Milli-Q water was added for overnight
557 equilibration (starvation). The water was removed from the equilibrated culture and replaced by 100µl
558 elicitor, supplemented with 50ng diaminofluorescein-FM diacetate (DAF-FM DA) (CAS: 254109-22-3)
559 (D23844; Invitrogen, CA, USA) to detect NO production. The elicitors used were 0.01% w/v glucose; 0.01%
560 w/v sucrose; 0.01% w/v glutamate; 0.01% w/v arginine; 0.01% w/v potassium nitrate; 0.01% w/v
561 potassium nitrite; sterile Milli-Q water; 100 ng mL-1 full-length flagellin (FFLG) (containing 0.01% sucrose;
562 tlrl-pstfla; Invivogen, CA, USA); 50 µg mL-1 lipooligosaccharides (LOS; LPS without the O-antigen), [92,93]; 50
563 µg mL-1 peptidoglycan (PGN) [94]; 100 nM flagellin 22 (Peptron Inc., South Korea); 100 nM elongation factor
564 18 (Peptron Inc., South Korea). We chose to use the 22 amino acid peptide from flagellin (FLG22) and the
565 18 amino acid from elongation factor Tu (EF-Tu; EF18), because they are known to be the epitopes that

elicit innate immunity in plants [6]. Fluorescence per well was measured in a 4x4 matrix (1400 gain) using a FLUOstar OPTIMA plate reader (BMG Labtech, Ortenberg, Germany) with emission filters at 485 nm and an excitation filter at 520 nm. Measurements were taken every 30 minutes for the duration of the experiment. The basal fluorescence reading (T0) at the start of the experiment was used as the control unless stated otherwise. The accumulation of NO as histograms is reported with readings at 10hr (T10) post elicitation or as graphs of accumulated fluorescence from produced NO. FFLG containing 0.01% sucrose was the most consistent inducer of NO and was used as a positive control in all the subsequent experiments. The germination time of the spores was challenging to replicate between experiments even if the culture producing the spores was grown similarly. Thus, the mycelial mats could be of different densities between the plates. All experiment treatments with controls (N=3 or more) and replicates (N=3 or more) were accommodated on one 96-welled healthy plate to compensate for that. In addition, the plates were first investigated for uniformity of the mycelial well development in all wells due to eventual pipetting handling mistakes (it should be the same absorbance from the fungal mat in all wells at the start of the experiment). The same was done for the other plate-reader-based assays below.

NOS inhibition assays

The assays were performed as described above, but before elicitation, the culture was exposed to the inhibitors for 2 hours. Inhibitors used was [10mM L-NNA, NG-nitro-L-Arginine;L-N^G-Nitroarginine (80220, Cayman Chemicals, MI, USA), 100µM W7, N-(6-Aminohexyl)-5-chloro-1-naphthalenesulfonamide hydrochloride (A3281, Sigma, MO, USA); 500nM ZSTK474 (S1072, Selleckchem, TX, USA); 100nM Wortmannin (W1628, Sigma, MO, USA); 25nM BpV(HOpic) (203701, Calbiochem-Millipore, MA, USA)] and elicitation was done with flagellin (containing 0.01% sucrose). Calcium ions in the flagellin solution were chelated with EGTA (E3889, Sigma, MO, USA) before elicitation. After 10 hours post elicitation, the NO accumulated level was compared, using FFLG-untreated cultures as negative controls.

NOS spike assays

F. graminearum was cultured and elicited with flagellin (FFLG) as described above. Post elicitation, the chemical of choice [Arginine (A8094); Potassium Nitrate (P6030); Potassium Nitrite (60417) from Sigma] was added to a final concentration of 5mM per well. The increase or decrease in the production of NO was monitored. For sequential spiking assays with arginine and potassium nitrite, the first substrate was added at 4 hours and the second substrate 2 hours later, (i.e. at 6 hours).

Procedure to find a putative $FgNCP_{NO}$

This procedure is described in detail (**Supplementary File SF2)** and outlined here. A mouse iNOS was looked up at NCBI. The protein domains were identified using HMMER, and the NCP-part of the protein was used for a protein blast (NCBI) against the *F. graminearum* PH1 predicted proteins. Two good hits (FGSG_09786 and FGSG_08413) were found for putative NCP_{NO} proteins. If any of these produce NO, the NO producing gene is likely co-regulated with a nitric oxide dioxygenase (NOD) to protect against too much NO formed. Two putative NODs were found in *F. graminearum* PH1 (**Supplementary File SF2**). A transcriptome dataset for *F. graminearum* with complete transcriptomes obtained for many different bacterial MAMPs exposure conditions was used to investigate for co-regulation with the identified putative NODs to indicate which of the two putative NCP_{NO} proteins are most likely an NCP_{NO}. This dataset was previously partly published [81] and is now available in full (**Supplementary Data1**

609 https://figshare.com/s/4a02adb12cb48dba6d7a (reserved DOI: 10.6084/m9.figshare.12361823)). The gene
610 FGSG_09786 but not FGSG_08413 was co-regulated with both NODs (**Fig.3 and Supplementary File SF4**)
611 and is most likely the $FgNCP_{NO}$ taking part in NO production.

612

613 **Procedure to find a putative $FgCYP_{NO}$**

614 When the NCP responsible for NO production (FGSG_09786) had been knocked out, found to be
615 responsible for NO production (an NCP_{NO}) and localized to the ER, it was possible to look for a heme-
616 containing $FgCYP_{NO}$ that can work together with NCP_{NO} at the ER membrane. The genome of *F.*
617 *graminearum* PH1 contains numerous genes annotated as coding for heme-binding proteins. To get a
618 complete list, we searched the whole genome for heme-domain-containing proteins using the Batch
619 Conserved Domain search tool to identify all occurrence of putative domains
620 (https://www.ncbi.nlm.nih.gov/Structure/bwrpsb/bwrpsb.cgi). These search results (**Supplementary**
621 **Data2** https://figshare.com/s/a853e4ff951355eb0228 (reserved DOI: 10.6084/m9.figshare.12386501)) was
622 then searched for proteins predicted to be heme-binding, and these proteins were listed. All heme
623 proteins were then sorted after their co-regulation with the $FgNCP_{NO}$ (FGSG_09786) in the transcriptome
624 data set for *F. graminearum* exposed to bacterial MAMPs (**Supplementary File SF5**). FGSG_07925 was
625 found to be most correlated with $FgNCP_{NO}$ but was not predicted to localize to ER or had a deletion and
626 complementation phenotype that could be expected for a true $FgCYP_{NO}$ (**Fig. S6 and S7**). However, the ER
627 localized FgNCPNO was not correctly predicted by PSORTII (**Table S5**) but correctly predicted to localize to
628 the ER membrane by DeepLoc. Thus, we used DeepLoc to predict the protein localization of the most
629 correlated proteins predicted to be heme-binding (**Supplementary File SF5**) and found that FGSG_01000 is
630 the most likely $FgCYP_{NO}$. This procedure is described in more detail in the supplementary file
631 (**Supplementary File SF6**).

632

633 **Knockout and complementation of $FgNCP_{NO}$ (FGSG_09786) and $FgCYP_{NO}$ (FGSG_01000)**

634 A 932-bp fragment upstream of FGSG_09786 and an 1176-bp fragment downstream of FGSG_09786 were
635 amplified with specific primers to replace the $FgNCP_{NO}$ (FGSG_09786) gene (**Table S14**). FGSG_09786
636 replacement constructs were finally generated by a split-marker approach [95]. Subsequently, the resulting
637 constructs were transformed into protoplasts of the wild-type strain PH-1. Hygromycin-resistant
638 transformants were screened by PCR using two pairs of primers (**Table S14**). Deletion of FGSG_09786 was
639 further verified by Southern blot with the Digoxigenin High Prime DNA Labeling and Detection Starter Kit I
640 (Roche, Mannheim, Germany). Using a similar strategy, $FgCYP_{NO}$ (FGSG_01000), two $FgNCP_{NO}$ (FGSG_00765,
641 FGSG_04458) and the first suspected $FgCYP_{NO}$ (FGSG_07925) deletion mutants were constructed. All
642 primers used in this study are listed in **Table S14**. At least two positive transformants for every gene were
643 used for phenotypic analyses. The primers FGSG_09786CF and FGSG_09786CR (**Table S14**) were used to
644 amplify the full-length sequence of the FGSG_09786 gene and its native promoter from the WT genomic
645 DNA to generate a pFGSG_09786-GFP fusion vector. It was then cloned into a pKNTG vector using the One
646 Step Cloning Kit (Vazyme Biotech Co., Ltd, China). The same method was used to construct pFGSG_00765-
647 GFP and pFGSG_04458-GFP and pFGSG_07925-GFP vectors using their respective primers. The primers
648 Mouse-09786-F and Mouse-09786-R (**Table S14**) were used to amplify the cDNA sequence of the
649 NM_008898 gene, and the primers FGSG_09786 promoter-F and FGSG_09786 promoter-R were used to
650 amplify the promoter of the FGSG_09786 gene to generate a heterologous complementary vector from
651 the mouse genome. Subsequently, the two fragments were fused and cloned into a pKNTG vector using
652 the One Step Cloning Kit (Vazyme Biotech Co., Ltd, China).

653

654 **Preparation of OMVs as MAMPs source for NO production**

655 Outer membrane vesicles carrying MAMPs are shed by Gram-negative bacteria [96,97]. OMVs were harvested
656 in the following way: An inoculum of *Escherichia coli* DH5α was inoculated to 10 ml 1/10 DFM medium [81] in
657 a 50ml in a sterilized centrifuge tube and incubated overnight at 28ºC. The bacterial cell culture was
658 harvested by centrifugation at 4200g for 5 minutes. The supernatant was removed, and the pellet washed
659 by being resuspended in 10 ml sterile MilliQ water. This washing was repeated twice. Finally, the pellet was
660 resuspended in 1 ml Milli Q water and incubated at 28ºC for 1 hour to allow OMVs to form. After
661 incubation, the suspension was harvested for OMVs by sterile filtration using a sterile 0.2 μm pore size
662 filter. The resulting liquid containing OMVs was used for MAMP treatments.

663

664 **NO measurements using mycelial plugs**

665 Milli Q water agar [81] was poured into a sterile Omnitray (Nunc), which is in principle a microtiter plate with
666 one 8x12 cm big rectangular well [98]. Fungal cultures of strains to be tested were grown on 1/10 DFM
667 medium in 9 cm diameter Petri dishes containing 10 ml DFM agar medium (Ipcho *et al.*, 2016). When
668 fungal mycelium was tested for NO production, 5 mm diameter plugs were cut away from the edge of the
669 mycelium to avoid getting DFM nutrients interfering with test [99]. A DAF-FM DA (ThermoFisher, D23844)
670 staining solution was prepared as 2 μl/ml of a stock solution (2 μg/μl in DMSO) was added to the bacterial
671 MAMPs suspension of OMVs or Milli Q water, giving a final concentration of 4 μg/ml DAF-FM DA. Droplets
672 (10 μl) of the DAF-FM DA staining solution with or without bacterial MAMPs were added on top of the
673 water agar in the Omnitray to perform the assay. Agar plugs were immediately put mycelium down on top
674 of the droplets, one agar plug per droplet. In each Omnitray, there was space for 4 rows of 4 replicate
675 plugs. *F. graminearum* PH1 was always used as positive and negative control taking up 2 rows to be
676 compared with mutant or complement strains with or without bacterial MAMPs in the remaining two
677 rows.

678 The amount of fluorescence from DAF-FM resulting from its reaction with NO was recorded for the whole
679 plate automatically (using the GFP-filter of the instrument) at roughly 0.5 h intervals. Recordings were
680 made through the plate's bottom, and a lid was kept on to avoid the plate's drying. The plate reader was
681 set up to produce one big image for the whole plate that could be exported as a TEXT image and imported
682 into the freeware ImageJ to produce a TIFF Z-stack that can be measured for the fluorescence
683 development over time in any defined area [98,100]. The fluorescence increase from each agar plug's hyphae
684 could then be analyzed and compared. For the first hours, the increase in fluorescence was linear,
685 indicating a linear accumulation of fluorescent DAF-FM products due to a constant NO production rate.
686 The curves' slope was used as relative measures of the NO formation rates to compare MAMPs treatments
687 with controls. The slopes for the fluorescence MAMPs/Water increase over time were used to compare
688 the strains' relative NO response to the MAMP treatments.

689

690 **Subcellular localization of NO production and measurements of NO production over time using confocal**
691 **microscopy using the NO probe DAF-FM DA**

692 NO was produced by *F. graminearum* PH1 mycelium also without MAMPs addition only a bit slower. DAF-
693 FM DA was added directly to a microscope slide to localise the intracellular sites of NO production.
694 Preliminary experiments showed that colour development was rapid. That was good since fluorescein
695 derivates like the resulting DAF-FM will quickly leak out or move to the vacuole as typical for fluorescein.

696 Therefore, we tried to minimize the time from adding DAF-FM DA to microscopy to get as good localization
697 as possible while still getting a good signal. Thus we picked fresh mycelium from a colony grown in a CM
698 agar medium and transferred that to a microscope slide, and added 10 μl water containing 2 μl DAF-FM DA
699 solution to a final concentration of 4 μg/ml and immediately observed for NO production localization
700 under a Nikon A1 confocal microscope for subcellular localization in NO production. Since we knew that
701 $FgNCP_{NO}$ responsible for NO production localizes to the ER (**Fig. 5B**), we used an *F. graminearum* strain
702 carrying a mCherry tagged ER-marker protein (ER-mCherry-HDEL) [101] to confirm that NO is formed at the
703 ER where the NO-forming proteins are localized (**Fig. 5C**).

704 Looking at the microscope images, it was evident that there were specks of autofluorescence that could
705 interfere with the DAF-FM signal. We chose to use the confocal microscope as a fluorimeter to avoid these
706 problems and get an alternative method for measuring NO formation from FgNCPNO and FgCYPNO. Slides
707 were prepared as above. Analysis method: A time series of images of the mycelium was recorded using a
708 10X objective for the GFP signal and the DIC signal. First, Import the ND2 time series Z-stack into ImageJ as
709 separate Tiff images, then separate GFP images and DIC images into folders and rename images so the
710 number order index comes first in the name, and import these image folders as separate 16-bit TIFF black
711 and white images into the freeware ImageJ (NIH, https://imagej.nih.gov/ij) to make two TIFF Z stacks.
712 Define a measured area (Region of Interest, ROI) in the DIC image that does not contain air bubbles but
713 relatively many hyphae. Import the ROI to the fluorescence image and check that there are no
714 autofluorescence specs (dots that do not fade with time) in this ROI. Do the same for an area without
715 hyphae as close to the previous area as possible to get a background control area. Measure and record the
716 Z-profile for the fluorescence in the measured area and the control area. Use the edge filter to transform
717 the DIC image to an image where the average light intensity is proportional to the biomass [102] and measure
718 and record this for the first image in the sequence (there is no change over time for the DIC image). To
719 maximize the analysis's sensitivity, we calculated the area under the fitted decay curve corrected for the
720 biomass measured from the DIC images as indicated above and used that as a relative measure for the NO
721 formation/biomass for the PH1, $FgNCP_{NO}$ and $FgCYP_{NO}$ (**Fig. 7A**).

722 Measurements of the NO formation of NO formation in the NCP-complements using the native
723 $FgNCP_{NO,TRI,ERG}$-GFP, or a Mouse-GFP orthologue created new problems. Both the DAF-FM signal and the
724 GFP signal are green. However, the pH-sensitive GFP signal fades very slowly and reproducibly in a
725 buffered environment (pH7) since blue light damage to membranes will not affect the fluorescence by pH
726 changes due to membrane leakages. Under similar conditions, the green DAF-FM signal fades entirely
727 within minutes of observation (**Supplementary Fig. S11 B**). This complete fading of the DAF-FM signal
728 makes it possible to reconstruct both the DAF-FM signal and the GFP signal at the start of the time
729 sequence and show these as full images (**Supplementary Fig. S11 A**). We made these new measurements
730 directly on agar slide cultures, making it easier to avoid air bubbles. The relative specific activity (NO signal
731 per protein GFP signal) of the two NCPs could thus be compared (**Supplementary Fig. S11 C**).

732

733 **Colony growth, conidiation, sexual reproduction, pathogenicity and DON production phenotypes**

734 Infection assays on flowering wheat heads and coleoptiles of cultivar XiaoYan 22 were conducted as
735 described previously [103,104]. For assaying DON production, fungal cultures were grown for 7 days at 25°C in
736 liquid trichothecene biosynthesis (LTB) medium [105]. Subsequently, a competitive enzyme-linked
737 immunosorbent assay (ELISA)-based DON detection plate kit (Beacon Analytical Systems, Saco, ME, USA)
738 was used to measure DON production. Growth rates were measured on complete medium (CM) plates and
739 conidiation assayed in liquid carboxymethyl cellulose (CMC) medium as described previously [106]. The
740 formation of perithecia was tested on carrot agar medium [107].

741

742 **Endocytosis assay using FM4-64**

743 Agar blocks (5 mm in diameter) were transferred from CM solid medium to 50ml centrifuge tubes
744 containing CM liquid medium. After 24h shaking, 10 µl of the fungal hyphae suspension was mixed with
745 FM4-64 to a final concentration of 4 µg/ml. Endocytosis of the stain was observed using a Nikon A1
746 confocal microscope using settings for TRITC (Fig. 11A). Endocytosis was estimated 1h after stain addition
747 when most of the FM4-64 stain had been endocytosed and distributed to intracellular organelles if
748 endocytosis is not blocked.

749

750 **Comparing $FgCYP_{NO}$ and $FgNCP_{NO}$ like proteins in eukaryotes, describing the domain structure and**
751 **predicting CaM binding**

752 These comparisons are described in detail (**Supplementary File SF7 and SF8)** and outlined here. First, NCBI
753 was blast-searched for all predicted proteins in Eukaryotes, similar to $FgNCP_{NO}$. From this result, a set of
754 organisms were selected that had good hits for the protein's whole length. Representative species were
755 chosen taxonomically closely related to *F. graminearum* and progressively further away as long as good
756 orthologues was found. The best hits were chosen, and phylogenetic trees for both proteins were
757 generated (**Fig. 9**). DeepLoc was in addition used to check that all similar proteins are predicted to localize
758 to ER and CaMELS (CalModulin intEraction Learning System) https://camels.pythonanywhere.com/) was
759 used to find likely CaM binding sites, while HMMER was used to predict domain structure and membrane
760 attachement for all these proteins (**Supplementary File SF7 and SF8).** All proteins were found to attach to
761 the the ER membrane with their N-terminal, have similar domains, domain order, very similar domain
762 sizes, and even distances between domains (**Fig. 10**).

763

764 **Statistics**

765 MS Excel was used to calculate the statistics presented in the figures. We have, were relevant, chosen to
766 use 95% confidence interval bars (SEM times 1.96) instead of standard t-tests to compare with controls
767 since it simplifies for the reader and is more stringent. Thus, bars with non-overlapping 95% confidence
768 intervals are significantly different (P-value for null hypothesis < 0.05).

769

770 Acknowledgements

771 Thanks to Professor Peter Stougaard, Department of Environmental Science. Environmental Microbiology
772 and Circular Resource Flow, Aalborg University, Denmark, for the initial discussions at the start of the work.
773 The Minnesota Supercomputing Institute is kindly acknowledged for computing resources and support for
774 producing the transcriptomic data for the fungus interacting with bacterial MAMPs [81] that was essential for
775 the study. We also thank The Velux Foundation (Denmark), which financed the initial Copenhagen part of
776 the research. We want to thank Dr Qiurong Xie from Fujian University of Traditional Chinese Medicine for
777 providing us with the cDNA for the mouse gene.

778

779 **Conflict of interest statement:** The authors declare they have no conflict of interest.

Data availability statement: All data used for this study are available as images or in supplemental files.

783 # References

784 1. Liu, X. *et al.* Diffusion-limited Reaction of Free Nitric Oxide with Erythrocytes. *Journal of Biological*
785 *Chemistry* **273**, 18709–18713 (1998).
786 2. Velayutham, M. & Zweier, J. L. Nitric Oxide Signaling in Biology. *messenger* **2**, 1–18 (2013).
787 3. Yu, M., Lamattina, L., Spoel, S. H. & Loake, G. J. Nitric oxide function in plant biology: a redox cue in
788 deconvolution. *New Phytol* **202**, 1142–1156 (2014).
789 4. Zeidler, D. Innate immunity in Arabidopsis thaliana: Lipopolysaccharides activate nitric oxide synthase
790 (NOS) and induce defense genes. *PLANT BIOLOGY* 6 (2004).
791 5. Ulett, G. & Potter, A. Nitric oxide and gram-positive pathogens: host triggers and bacterial defence
792 mechanisms. in *Stress response in pathogenic bacteria* (ed. Kidd, S. P.) 68–89 (CABI, 2011).
793 doi:10.1079/9781845937607.0068.
794 6. Newman, M.-A., Sundelin, T., Nielsen, J. T. & Erbs, G. MAMP (microbe-associated molecular pattern)
795 triggered immunity in plants. *Front. Plant Sci.* **4**, (2013).
796 7. Stuehr, D. J. Mammalian nitric oxide synthases. *Biochimica et Biophysica Acta* **1411**, 217–230 (1999).
797 8. Gorren, A. C. F. & Mayer, B. Nitric-oxide synthase: A cytochrome P450 family foster child. *Biochimica et*
798 *Biophysica Acta (BBA) - General Subjects* **1770**, 432–445 (2007).
799 9. Abu-Soud, H. M., Ichimori, K., Nakazawa, H. & Stuehr, D. J. Regulation of Inducible Nitric Oxide
800 Synthase by Self-Generated NO. *Biochemistry* **40**, 6876–6881 (2001).
801 10. Bogdan, C., Rollinghoff, M. & Diefenbach, A. The role of nitric oxide in innate immunity. *Immunol Rev*
802 **173**, 17–26 (2000).
803 11. Erez, A. *et al.* Requirement of argininosuccinate lyase for systemic nitric oxide production. *Nat Med* **17**,
804 1619–1626 (2011).
805 12. Fröhlich, A. & Durner, J. The hunt for plant nitric oxide synthase (NOS): Is one really needed? *Plant*
806 *Science* **181**, 401–404 (2011).
807 13. Rőszer, T. *The biology of subcellular nitric oxide*. (Springer, 2012).

808 14. Samalova, M. *et al.* Nitric oxide generated by the rice blast fungus *Magnaporthe oryzae* drives plant
809 infection. *New Phytol* **197**, 207–222 (2013).
810 15. Guo, F.-Q. Identification of a Plant Nitric Oxide Synthase Gene Involved in Hormonal Signaling. *Science*
811 **302**, 100–103 (2003).
812 16. Guo, F.-Q. & Crawford, N. M. *Arabidopsis* Nitric Oxide Synthase1 Is Targeted to Mitochondria and
813 Protects against Oxidative Damage and Dark-Induced Senescence. *Plant Cell* **17**, 3436–3450 (2005).
814 17. Hong, J. K. *et al.* Nitric oxide function and signalling in plant disease resistance. *Journal of Experimental*
815 *Botany* **59**, 147–154 (2008).
816 18. Moreau, M., Lee, G. I., Wang, Y., Crane, B. R. & Klessig, D. F. AtNOS/AtNOA1 Is a Functional *Arabidopsis*
817 *thaliana* cGTPase and Not a Nitric-oxide Synthase. *J. Biol. Chem.* **283**, 32957–32967 (2008).
818 19. Kanadia, R. N., Kuo, W. N., Mcnabb, M. & Botchway, A. Constitutive nitric oxide synthase in
819 *Saccharomyces cerevisiae*. *TBMB* **45**, 1081–1087 (1998).
820 20. Domitrovic, T. *et al.* Role of nitric oxide in the response of cells to heat shock and high hydrostatic
821 pressure. *FEMS Yeast Research* **3**, 341–346 (2003).
822 21. Wang, J. & Higgins, V. J. Nitric oxide has a regulatory effect in the germination of conidia of
823 *Colletotrichum coccodes*. *Fungal Genetics and Biology* **42**, 284–292 (2005).
824 22. Gong, X. *et al.* l-Arginine is essential for conidiation in the filamentous fungus *Coniothyrium minitans*.
825 *Fungal Genetics and Biology* **44**, 1368–1379 (2007).
826 23. Prats, E., Carver, T. L. W. & Mur, L. A. J. Pathogen-derived nitric oxide influences formation of the
827 appressorium infection structure in the phytopathogenic fungus *Blumeria graminis*. *Research in*
828 *Microbiology* **159**, 476–480 (2008).
829 24. Rockel, P., Strube, F., Rockel, A., Wildt, J. & Kaiser, W. M. Regulation of nitric oxide (NO) production by
830 plant nitrate reductase in vivo and in vitro. *Journal of Eperimental Botany* **53**, 103–110 (2002).
831 25. Jansson, E. Å. *et al.* A mammalian functional nitrate reductase that regulates nitrite and nitric oxide
832 homeostasis. *Nat Chem Biol* **4**, 411–417 (2008).

833 26. Lundberg, J. O. *et al.* Nitrate and nitrite in biology, nutrition and therapeutics. *Nat Chem Biol* **5**, 865–
834 869 (2009).
835 27. Lozano-Juste, J. & León, J. Enhanced Abscisic Acid-Mediated Responses in *nia1nia2noa1-2* Triple
836 Mutant Impaired in NIA/NR- and AtNOA1-Dependent Nitric Oxide Biosynthesis in Arabidopsis. *Plant*
837 *Physiol.* **152**, 891–903 (2010).
838 28. Tejada-Jimenez, M., Llamas, A., Galván, A. & Fernández, E. Role of Nitrate Reductase in NO Production
839 in Photosynthetic Eukaryotes. *Plants* **8**, 56 (2019).
840 29. Ding, Y., Gardiner, D. M., Xiao, D. & Kazan, K. Regulators of nitric oxide signaling triggered by host
841 perception in a plant pathogen. *Proc Natl Acad Sci USA* **117**, 11147–11157 (2020).
842 30. Marcos, A. T. *et al.* Nitric oxide synthesis by nitrate reductase is regulated during development in *A*
843 *spergillus*. *Molecular Microbiology* **99**, 15–33 (2016).
844 31. Cavinder, B., Sikhakolli, U., Fellows, K. M. & Trail, F. Sexual Development and Ascospore Discharge in
845 *Fusarium graminearum*. *Journal of Visualized Experiments* (2012) doi:10.3791/3895.
846 32. Wang, Q., Vera Buxa, S., Furch, A., Friedt, W. & Gottwald, S. Insights Into *Triticum aestivum* Seedling
847 Root Rot Caused by *Fusarium graminearum*. *MPMI* **28**, 1288–1303 (2015).
848 33. Ipcho, S. *et al.* Fungal Innate Immunity Induced by Bacterial Microbe-Associated Molecular Patterns
849 (MAMPs). *G3; Genes|Genomes|Genetics* **6**, 1585–1595 (2016).
850 34. Zipfel, C. & Felix, G. Plants and animals: a different taste for microbes? *Current Opinion in Plant Biology*
851 **8**, 353–360 (2005).
852 35. Kikuchi, K. & Nagano, T. Detection of Nitric Oxide Production from a Perfused Organ by a Luminol-
853 H202 System. *Analytical Chemistry* **65**, 1794–1799 (1993).
854 36. Günzl, P. & Schabbauer, G. Recent advances in the genetic analysis of PTEN and PI3K innate immune
855 properties. *Immunobiology* **213**, 759–765 (2008).
856 37. Ma, W., Smigel, A., Tsai, Y.-C., Braam, J. & Berkowitz, G. A. *Plant Physiol.* **148**, 818–828 (2008).
857 38. Mori, M. & Gotoh, T. Arginine Metabolic Enzymes, Nitric Oxide and Infection. *The Journal of Nutrition*
858 **134**, 2820S-2825S (2004).

859 39. Lee, S.-J. & Stull, J. T. Calmodulin-dependent Regulation of Inducible and Neuronal Nitric-oxide
860 Synthase. *J. Biol. Chem.* **273**, 27430–27437 (1998).
861 40. Li, N., Sul, J.-Y. & Haydon, P. G. A Calcium-Induced Calcium Influx Factor, Nitric Oxide, Modulates the
862 Refilling of Calcium Stores in Astrocytes. *J. Neurosci.* **23**, 10302–10310 (2003).
863 41. Nagpal, L. & Panda, K. Characterization of Calmodulin-Free Murine Inducible Nitric-Oxide Synthase.
864 *PLoS ONE* **10**, e0121782 (2015).
865 42. Cánovas, D., Marcos, J. F., Marcos, A. T. & Strauss, J. Nitric oxide in fungi: is there NO light at the end of
866 the tunnel? *Curr Genet* **62**, 513–518 (2016).
867 43. Crane, B. R. Structure of Nitric Oxide Synthase Oxygenase Dimer with Pterin and Substrate. *Science*
868 **279**, 2121–2126 (1998).
869 44. Gardner, P. R. Hemoglobin: A Nitric-Oxide Dioxygenase. *Scientifica* **2012**, 1–34 (2012).
870 45. Missall, T. A., Lodge, J. K. & McEwen, J. E. Mechanisms of Resistance to Oxidative and Nitrosative
871 Stress: Implications for Fungal Survival in Mammalian Hosts. *Eukaryotic Cell* **3**, 835–846 (2004).
872 46. Jian, Y. *et al.* Interplay of two transcription factors for recruitment of the chromatin remodeling
873 complex modulates fungal nitrosative stress response. *Nat Commun* **12**, 2576 (2021).
874 47. Proctor, R. H., Hohn, T. M. & McCormick, S. P. Reducend Virulence of *Gibberella zea* Caused by
875 Disruption of Trichothecene Biosynthetic Gene. *MPMI* **8**, 593–601 (1995).
876 48. Almagro Armenteros, J. J., Sønderby, C. K., Sønderby, S. K., Nielsen, H. & Winther, O. DeepLoc:
877 prediction of protein subcellular localization using deep learning. *Bioinformatics* **33**, 3387–3395 (2017).
878 49. Kim, H.-S. *et al.* Roles of three *Fusarium graminearum* membrane Ca^{2+}) channels in the formation of
879 Ca^{2+}) signatures, growth, development, pathogenicity and mycotoxin production. *Fungal Genetics and*
880 *Biology* **111**, 30–46 (2018).
881 50. Abbasi, W. A., Asif, A., Andleeb, S. & Minhas, F. ul A. A. CaMELS: In silico prediction of calmodulin
882 binding proteins and their binding sites. *Proteins* **85**, 1724–1740 (2017).
883 51. Lepesheva, G. I. & Waterman, M. R. Sterol 14α-demethylase cytochrome P450 (CYP51), a P450 in all
884 biological kingdoms. *Biochimica et Biophysica Acta (BBA) - General Subjects* **1770**, 467–477 (2007).

885 52. Kim, J. H., Singh, A., Del Poeta, M., Brown, D. A. & London, E. The effect of sterol structure upon
886 clathrin-mediated and clathrin-independent endocytosis. *J Cell Sci* **130**, 2682–2695 (2017).
887 53. Suchodolski, J., Muraszko, J., Bernat, P. & Krasowska, A. A Crucial Role for Ergosterol in Plasma
888 Membrane Composition, Localisation, and Activity of Cdr1p and H^+-ATPase in Candida albicans.
889 *Microorganisms* **7**, 378 (2019).
890 54. Zhang, L. *et al.* Conserved Eukaryotic Kinase CK2 Chaperone Intrinsically Disordered Protein
891 Interactions. *Appl Environ Microbiol* **86**, e02191-19, /aem/86/2/AEM.02191-19.atom (2019).
892 55. Tokai, T. *et al.* Fusarium Tri4 encodes a key multifunctional cytochrome P450 monooxygenase for four
893 consecutive oxygenation steps in trichothecene biosynthesis. *Biochemical and Biophysical Research*
894 *Communications* **353**, 412–417 (2007).
895 56. Kistler, H. C. & Broz, K. Cellular compartmentalization of secondary metabolism. *Front. Microbiol.* **6**, 1–
896 11 (2015).
897 57. Arrua Alvarenga, A. A. *et al.* Trichothecene Genotype Profiling of Wheat Fusarium graminearum
898 Species Complex in Paraguay. *Toxins* **14**, 257 (2022).
899 58. Stuchebrukhov, A. A. Long-distance electron tunneling in proteins: A new challenge for time-resolved
900 spectroscopy. *Laser Phys.* **20**, 125–138 (2010).
901 59. Fereiro, J. A. *et al.* Tunneling explains efficient electron transport via protein junctions. *Proc Natl Acad*
902 *Sci USA* **115**, E4577–E4583 (2018).
903 60. Chen, K., Pittman, R. N. & Popel, A. S. Nitric Oxide in the Vasculature: Where Does It Come From and
904 Where Does It Go? A Quantitative Perspective. *Antioxidants & Redox Signaling* **10**, 1185–1198 (2008).
905 61. Andronik-Lion, V., Boucher, J. L., Delaforge, M., Henry, Y. & Mansuy, D. Formation of nitric oxide by
906 cytochrome P450-catalyzed oxidation of aromatic amidoximes. *Biochemical and Biophysical Research*
907 *Communications* **185**, 452–458 (1992).
908 62. Boucher, J.-L., Genet, A., Vadon, S., Delaforge, M. & Mansuy, D. Cytochrome P450 catalyzes the
909 oxidation of Nω-hydroxy-L-arginine by NADPH and O2 to nitric oxide and citrulline. *Biochem. Biophys.*
910 *Res. Commun.* **187**, 880–886 (1992).

911 63. Boucher, J. L., Genet, A., Vadon, S., Delaforge, M. & Mansuy, D. Formation of nitrogen oxides and
912 citrulline upon oxidation of Nω-hydroxy-L-arginine by hemeproteins. *Biochemical and Biophysical*
913 *Research Communications* **184**, 1158–1164 (1992).
914 64. Keserü, G. M., Volk, B. & Balogh, G. T. Cytochrome P450 Catalyzed Nitric Oxide Synthesis: A Theoretical
915 Study. *Journal of Biomolecular Structure and Dynamics* **17**, 759–767 (2000).
916 65. Chai, H. *et al.* Long Distance Electron Transfer Across >100 nm Thick Au Nanoparticle/Polyion Films to a
917 Surface Redox Protein. *Electroanalysis* **24**, 1129–1140 (2012).
918 66. Kuss-Petermann, M. & Wenger, O. S. Increasing Electron-Transfer Rates with Increasing Donor-
919 Acceptor Distance. *Angew. Chem. Int. Ed.* **55**, 815–819 (2016).
920 67. Etzerodt, T., Wetterhorn, K., Dionisio, G. & Rayment, I. Functional characterization of a soluble NADPH-
921 cytochrome P450 reductase from Fusarium graminearum. *Protein Expression and Purification* **138**, 69–
922 75 (2017).
923 68. Diamond, M. *et al.* The Fusarium Mycotoxin Deoxynivalenol Can Inhibit Plant Apoptosis-Like
924 Programmed Cell Death. *PLoS ONE* **8**, e69542 (2013).
925 69. Rauscher, R. & Ignatova, Z. Tuning innate immunity by translation. *Biochemical Society Transactions*
926 **43**, 1247–1252 (2015).
927 70. Lofgren, L. A. *et al. Fusarium graminearum:* pathogen or endophyte of North American grasses? *New*
928 *Phytol* **217**, 1203–1212 (2018).
929 71. Granado, J., Felix, G. & Boller, T. Perception of Fungal Sterols in Plants'. *Plant Physiology* **107**, 6 (1995).
930 72. Klemptner, R. L., Sherwood, J. S., Tugizimana, F., Dubery, I. A. & Piater, L. A. Ergosterol, an orphan
931 fungal microbe-associated molecular pattern (MAMP): Ergosterol as a MAMP. *Molecular Plant*
932 *Pathology* **15**, 747–761 (2014).
933 73. Liu, X. *et al.* Paralogous cyp51 genes in Fusarium graminearum mediate differential sensitivity to sterol
934 demethylation inhibitors. *Fungal Genetics and Biology* **48**, 113–123 (2011).
935 74. Kachroo, A. H. *et al.* Systematic humanization of yeast genes reveals conserved functions and genetic
936 modularity. *Science* **348**, 921–925 (2015).

937 75. Park, J. W., Byrd, A., Lee, C. & Morgan, E. T. Nitric oxide stimulates cellular degradation of human
938 CYP51A1, the highly conserved lanosterol 14α-demethylase. *Biochemical Journal* **474**, 3241–3252
939 (2017).
940 76. Martinez, I., Sveinbjørnsson, B. & Smedsrød, B. Nitric Oxide Down-Regulates Endocytosis in Rat Liver
941 Endothelial Cells. *Biochemical and Biophysical Research Communications* **222**, 688–693 (1996).
942 77. Pichler, H. & Riezman, H. Where sterols are required for endocytosis. *Biochimica et Biophysica Acta*
943 *(BBA) - Biomembranes* **1666**, 51–61 (2004).
944 78. Cuong, N. D. Isolation of efficient Burkholderia sp. strains to control Rhizoctonia solani (sheath blight)
945 in rice. (PhD Thesis, University of Copenhagen, Faculty of Life Sciences, Department of Agriculture and
946 Ecology, 2010).
947 79. Cuong, N. D., Nicolaisen, M. H., Sørensen, J. & Olsson, S. Hyphae-colonizing *Burkholderia* sp.—A New
948 source of biological control agents against sheath blight disease (*Rhizoctonia solani* AG1-IA) in rice.
949 *Microb Ecol* **62**, 425–434 (2011).
950 80. Nicolaisen, M. H. *et al.* Biological control of rice sheath blight using hyphae-associated bacteria:
951 development of an *in planta* screening assay to predict biological control agent performance under
952 field conditions. *BioControl* **63**, 843–853 (2018).
953 81. Ipcho, S. *et al.* Fungal Innate Immunity Induced by Bacterial Microbe-Associated Molecular Patterns
954 (MAMPs). *G3* **6**, 1585–1595 (2016).
955 82. Veiga, E. & Cossart, P. Listeria hijacks the clathrin-dependent endocytic machinery to invade
956 mammalian cells. *Nat Cell Biol* **7**, 894–900 (2005).
957 83. Herbert, K. E. & Erridge, C. Regulation of low-density lipoprotein cholesterol by intestinal inflammation
958 and the acute phase response. *Cardiovascular Research* **114**, 226–232 (2018).
959 84. Tamboli, I. Y. *et al.* Loss of -Secretase Function Impairs Endocytosis of Lipoprotein Particles and
960 Membrane Cholesterol Homeostasis. *Journal of Neuroscience* **28**, 12097–12106 (2008).
961 85. Hummel, S. G., Fischer, A. J., Martin, S. M., Schafer, F. Q. & Buettner, G. R. Nitric oxide as a cellular
962 antioxidant: A little goes a long way. *Free Radical Biology and Medicine* **40**, 501–506 (2006).

963 86. Dupont, S. *et al.* Antioxidant Properties of Ergosterol and Its Role in Yeast Resistance to Oxidation.
964 *Antioxidants* **10**, 1024 (2021).
965 87. Mostofian, B., Zhuang, T., Cheng, X. & Nickels, J. D. Branched-Chain Fatty Acid Content Modulates
966 Structure, Fluidity, and Phase in Model Microbial Cell Membranes. *J. Phys. Chem. B* **123**, 5814–5821
967 (2019).
968 88. Josefsen, L. *et al.* Autophagy provides nutrients for nonassimilating fungal structures and is necessary
969 for plant colonization but not for infection in the necrotrophic plant pathogen Fusarium graminearum.
970 *Autophagy* **8**, 326–337 (2012).
971 89. Luiking, Y. C., Poeze, M., Ramsay, G. & Deutz, N. E. Reduced citrulline production in sepsis is related to
972 diminished de novo arginine and nitric oxide production. *The American Journal of Clinical Nutrition* **89**,
973 142–152 (2009).
974 90. Tudzynski, B. Nitrogen regulation of fungal secondary metabolism in fungi. *Front. Microbiol.* **5**, (2014).
975 91. Yoder, W. T. & Christianson, L. M. Species-Specific Primers Resolve Members of *Fusarium* Section
976 *Fusarium*. Taxonomic Status of the Eible 'Quorn' Fungus Reevaluated. *Fungal Genetics and Biology* **23**,
977 68–80 (1998).
978 92. Silipo, A. *et al.* The Elicitation of Plant Innate Immunity by Lipooligosaccharide of *Xanthomonas*
979 *campestris*. *J. Biol. Chem.* **280**, 33660–33668 (2005).
980 93. Silipo, A. *et al.* Structural characterization of two lipopolysaccharide O-antigens produced by the
981 endofungal bacterium Burkholderia sp HKI-402 (B4). *Carbohyd Res* **347**, 95–98 (2012).
982 94. Erbs, G. *et al.* Peptidoglycan and Muropeptides from Pathogens Agrobacterium and Xanthomonas
983 Elicit Plant Innate Immunity: Structure and Activity. *Chemistry & Biology* **15**, 438–448 (2008).
984 95. Yu, J. *et al.* Double-joint PCR: a PCR-based molecular tool for gene manipulations in filamentous fungi.
985 *Fungal Genetics And Biology* **41**, 973–981 (2004).
986 96. Tashiro, Y. *et al.* Variation of Physiochemical Properties and Cell Association Activity of Membrane
987 Vesicles with Growth Phase in Pseudomonas aeruginosa. *Applied and Environmental Microbiology* **76**,
988 3732–3739 (2010).

989 97. Cecil, J., Sirisaengtaksin, N., O'Brien-Simpson, N. & Krachler, A. Outer Membrane Vesicle-Host Cell
990 Interactions. *Mikrobiol Spectrum* **7**, 11 (2019).
991 98. Hennessy, R. C., Stougaard, P. & Olsson, S. A Microplate Reader-Based System for Visualizing
992 Transcriptional Activity During in vivo Microbial Interactions in Space and Time. *Sci Rep* **7**, 281 (2017).
993 99. Olsson, S. Uptake of Glucose and Phosphorus by Growing Colonies of Fusarium-Oxysporum as
994 Quantified by Image-Analysis. *Exp Mycol* **18**, 33–47 (1994).
995 100. Hennessy, R., Stougaard, P. & Olsson, S. Imaging Gene Expression Dynamics in Pseudomonas
996 fluorescens In5 during Interactions with the Fungus Fusarium graminearum PH-1. *BIO-PROTOCOL* **9**,
997 (2019).
998 101. Adnan, M. *et al.* R-SNARE FgSec22 is essential for growth, pathogenicity and DON production of
999 Fusarium graminearum. *Curr Genet* **66**, 421–435 (2020).
1000 102. Olsson, S. Mycelial density profiles of fungi on heterogeneous media and their interpretation in
1001 terms of nutrient reallocation patterns. *Mycological Research* **99**, 143–153 (1995).
1002 103. Ding, S. *et al.* Transducin Beta-Like Gene *FTL1* Is Essential for Pathogenesis in *Fusarium*
1003 *graminearum*. *Eukaryotic Cell* **8**, 867–876 (2009).
1004 104. Zhang, X.-W. *et al.* In Planta Stage-Specific Fungal Gene Profiling Elucidates the Molecular
1005 Strategies of *Fusarium graminearum* Growing inside Wheat Coleoptiles. *Plant Cell* **24**, 5159–5176
1006 (2012).
1007 105. Jiang, C. *et al.* TRI6 and TRI10 play different roles in the regulation of deoxynivalenol (DON)
1008 production by cAMP signalling in *Fusarium graminearum*. *Environmental Microbiology* **18**, 3689–3701
1009 (2016).
1010 106. Zheng, W. *et al.* A conserved homeobox transcription factor Htf1 is required for phialide
1011 development and conidiogenesis in Fusarium species. *PLOS ONE* **7**, e45432 (2012).
1012 107. Wang, C. *et al.* Functional Analysis of the Kinome of the Wheat Scab Fungus *Fusarium*
1013 *graminearum*. *PLoS Pathog* **7**, e1002460 (2011).

1014 108. Kuss-Petermann, M. & Wenger, O. S. Increasing Electron-Transfer Rates with Increasing Donor-
1015 Acceptor Distance. *Angew. Chem. Int. Ed.* **55**, 815–819 (2016).
1016 109. Suchodolski, J., Muraszko, J., Bernat, P. & Krasowska, A. A Crucial Role for Ergosterol in Plasma
1017 Membrane Composition, Localisation, and Activity of Cdr1p and H+-ATPase in Candida albicans.
1018 *Microorganisms* **7**, 378 (2019).
1019 110. Martinez, I., Sveinbjørnsson, B. & Smedsrød, B. Nitric Oxide Down-Regulates Endocytosis in Rat
1020 Liver Endothelial Cells. *Biochemical and Biophysical Research Communications* **222**, 688–693 (1996).
1021 111. Souza, C. M. & Pichler, H. Lipid requirements for endocytosis in yeast. *Biochimica et Biophysica*
1022 *Acta (BBA) - Molecular and Cell Biology of Lipids* **1771**, 442–454 (2007).
1023 112. He, F. *et al.* Host-Induced Silencing of Fusarium graminearum Genes Enhances the Resistance of
1024 Brachypodium distachyon to Fusarium Head Blight. *Front. Plant Sci.* **10**, 1362 (2019).
1025 113. McCormick, S. P., Alexander, N. J. & Proctor, R. H. *Fusarium Tri4* encodes a multifunctional
1026 oxygenase required for trichothecene biosynthesis. *Can. J. Microbiol.* **52**, 636–642 (2006).
1027
1028

Figures and Tables

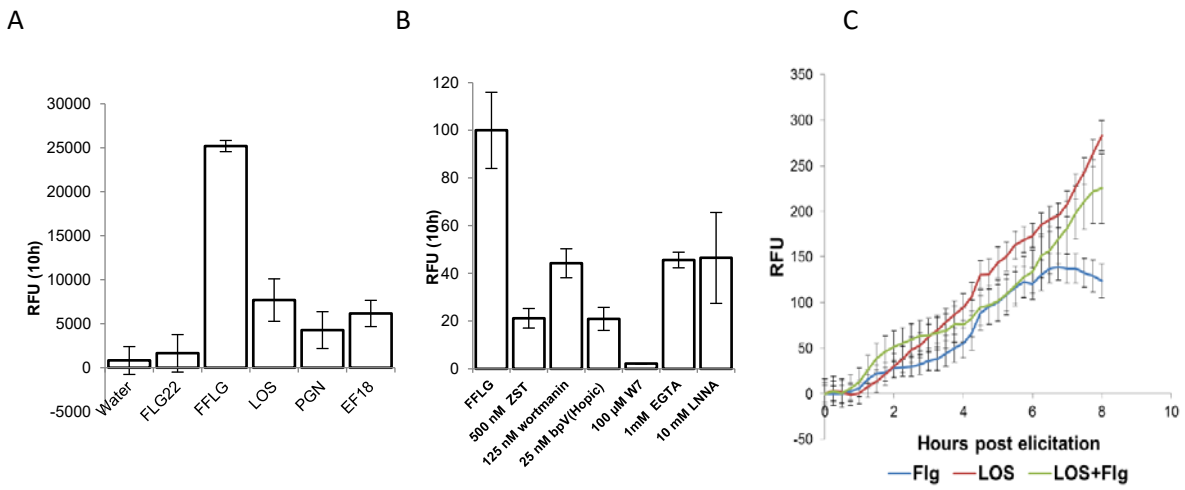

Figure 1. (**A**) Accumulated increased NO production measured as an increase of the NO probe DAF-FM DA's fluorescence during 10h post-stimulation by adding different bacterial MAMPs (Microbe Associated Molecular Patterns). Water was used as a negative control to test if the disturbance by addition triggers NO production. FLG22=the short flagellin peptide, plant flagellin receptors senses. FFLG=full length flagellin, LOS=lipo-oligosaccharides, PGN=peptidoglycan, EF18= Elongation factor 18. Three biological replicates were used, and error bars show 95% confidence intervals for the mean values. Thus, the P-value for the null hypothesis for the same average of bars with non-overlapping error bars <<0.05. (**B**) Accumulated relative increased NO production was measured as an increase of the NO probe DAF-FM DA fluorescence during 10 h post-stimulation by adding full-length flagellin (FFLG) as positive control with different inhibitors together with FFLG as treatments. FFLG=Full length flagellin, ZST=ZSTK474 PI3K inhibitor, wortmannin=PI3K inhibitor, bpV(Hopic)=PTEN inhibitor, W7=calmodulin inhibitor, EGTA=Calcium chelator, LNNA=L-N^G-nitro-L-arginine NOS inhibitor. Three biological replicates were used, and error bars show 95% confidence intervals for the mean values. Thus, the P-value for the null hypothesis for the same average of bars with non-overlapping error bars <<0.05. (**C**) The relative increase in fluorescence of the intracellular calcium probe Fluo4, that was directly added to the fungal biomass in the wells (1µg/ml), was subtracted for fluorescence in the negative control with only water. Error bars show the standard error of means (N=3).

1054 A B

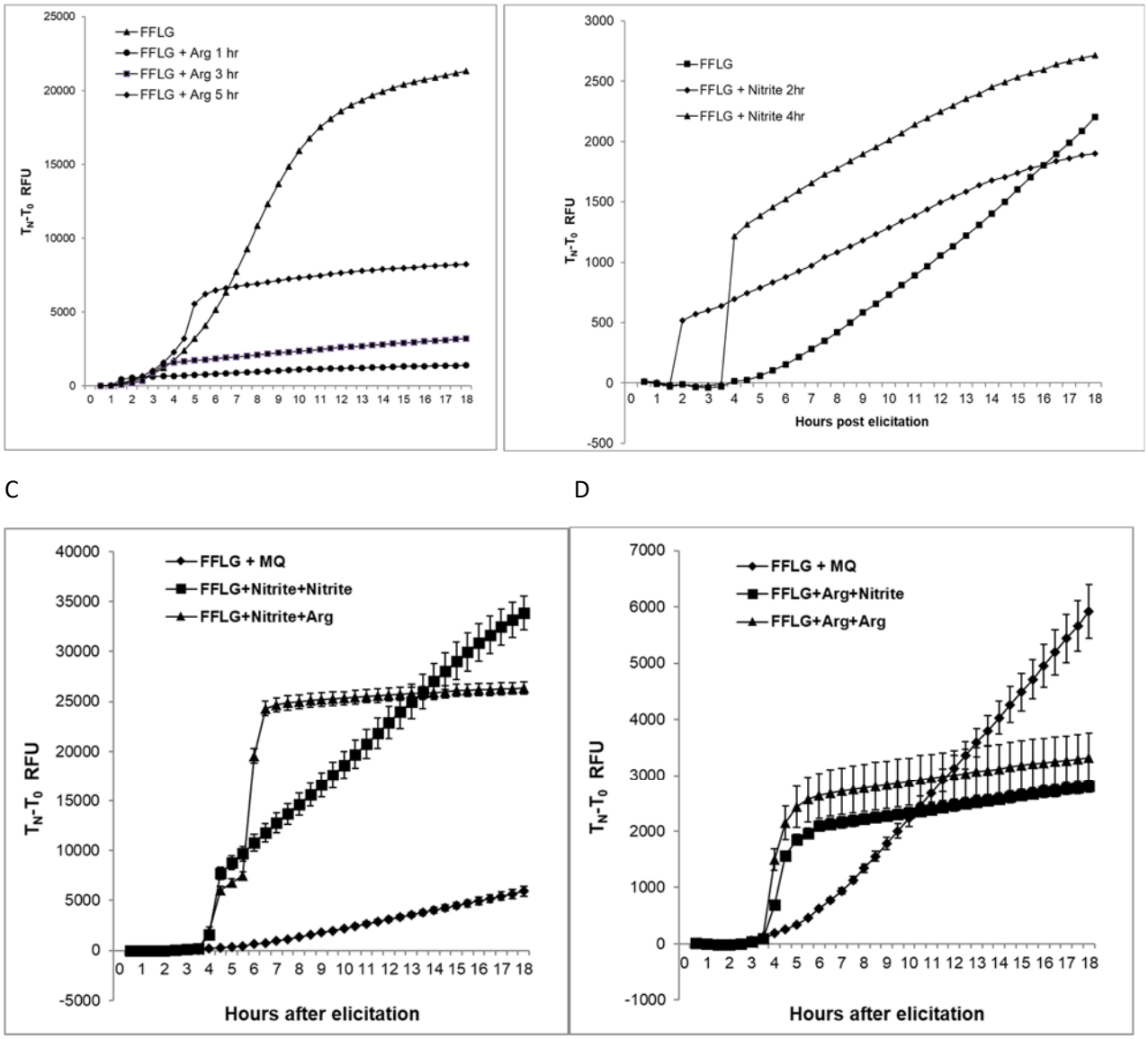

1055

1056 C D

1057

1058 **Figure 2.** (**A**) Effect on NO production in treatment minus control of adding exogenous arginine or (**B**)
1059 nitrite on NO production. Both were added to a final concentration of 5mM. The NO production rate
1060 increased very quickly after addition, and in the case of arginine, the rapid increase stopped accumulating
1061 soon after addition. The inhibition was less in the nitrite additions. (**C**) Sequential spiking nitrite and arginine to
1062 flagellin-induced fungal cultures. First, spiking by nitrite followed by a second nitrite spiking or an arginine spiking. (**D**)
1063 First, spiking arginine followed by arginine spiking or nitrite spiking. Arginine spiking limits total NO accumulation, but
1064 this does not happen with nitrite spiking. Error bars are standard errors of the mean (N=3). In A and B, no error bars
1065 are shown since they are small and hide the shapes of the curves.

1066

1067

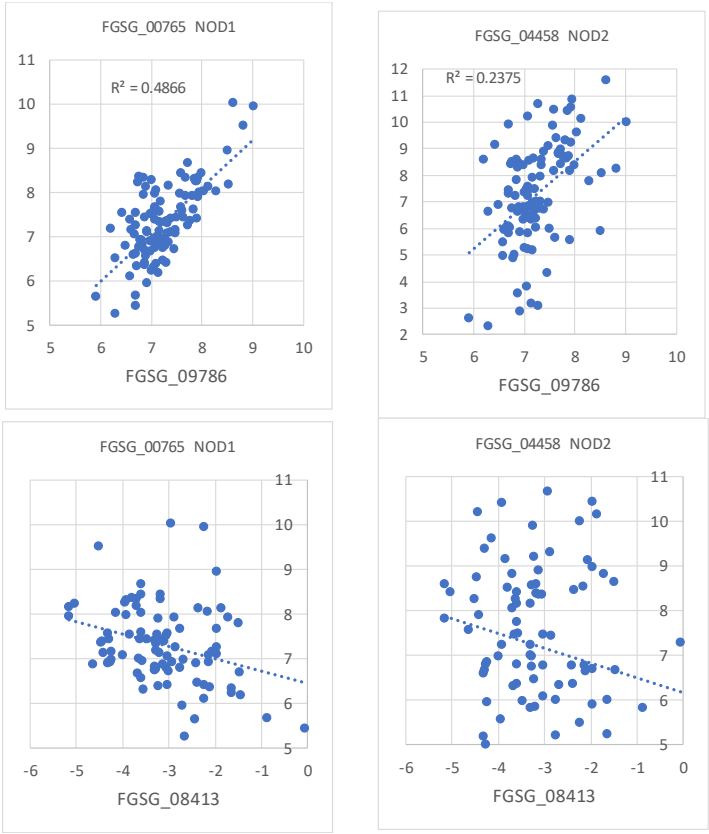

1068

1069 **Figure 3**. Correlations of expression between the two putative *FgNCP*$_{NO}$ (FGSG_09786 and FGSG_08413) and the two
1070 putative *FgNODs* (FGSG_00765 NOD1 and FGSG_04458 NOD2) in the transcriptome dataset for fungal interactions
1071 with bacterial MAMPs (see methods). FGSG_09786 is positively correlated with the *NOD* genes and is thus more likely
1072 to take part in producing NO. Log2 values for the relative expression are used for both axes, and scales for both axes
1073 are set the same to aid visual comparisons. N=108.

1074

1075

1076 A B

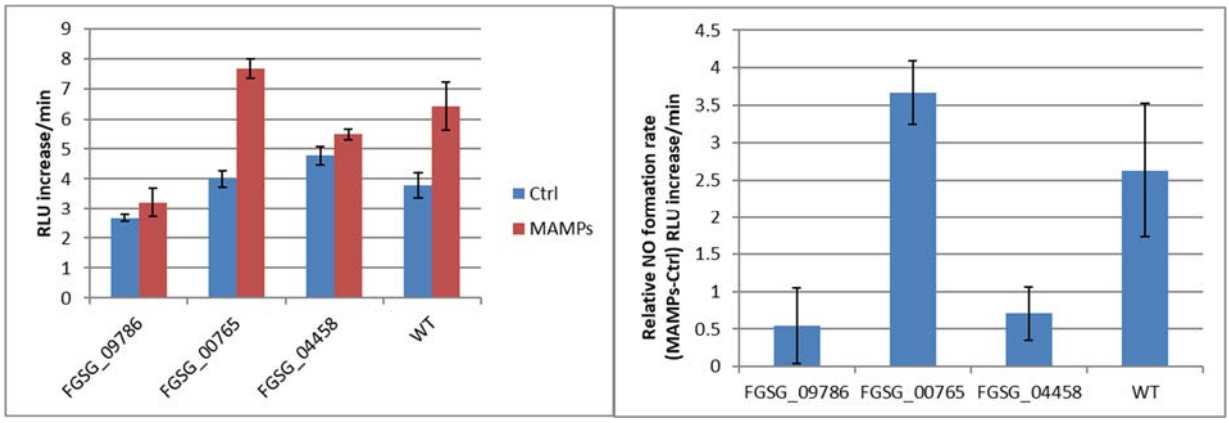

1077

1078 **Figure 4. (A)** Relative increase rate in fluorescence units of the NO probe DAF-FM per minute in water controls
1079 hyphae treated with bacterial MAMPs (sterile bacterial washings, see methods). (**B**) The same data was normalized by
1080 their respective water controls. The results show that FGSG_09786 is the sought for *FgNCP*$_{NO}$ and, of the two putative
1081 FgNODs, FGSG_00765 is more likely the NOD counterpart limiting NO production. FGSG_09786=*ΔFgNCP*$_{NO}$,
1082 FGSG_00765= *ΔFgNOD1* and FGSG_04458=*ΔFgNOD2.* Four replicates were used, and error bars show 95%
1083 confidence intervals for the mean values. Thus, the P-value for the null hypothesis for the same average of bars with
1084 non-overlapping error bars <<0.05.

1085

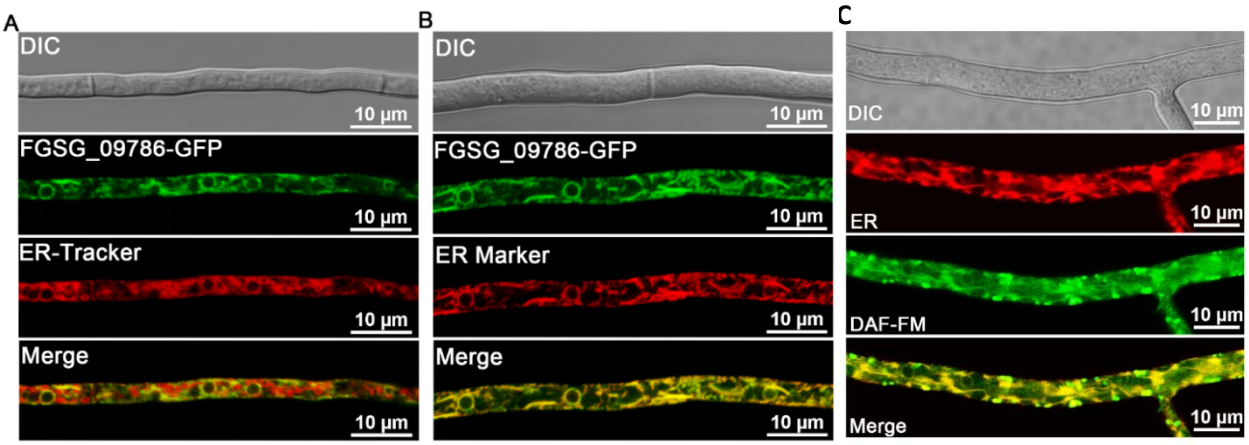

Figure 5. (**A**) Cellular localization of $FgNCP_{NO}$ (FGSG_09786) in hyphae of *F. graminearum* compared with the localization of an ER-tracker often used to label ER but with less specificity than (**B**) mCherry labelled ER Marker protein (see methods). (**C**) Localization of NO signal (DAF-FM) compared with the localization of the ER Marker protein (ER). The results show that the $FgNCP_{NO}$ (FGSG_09786) localizes to the ER, where the NO is mainly produced.

1112

1113

1114

1115

1116

1117

1118

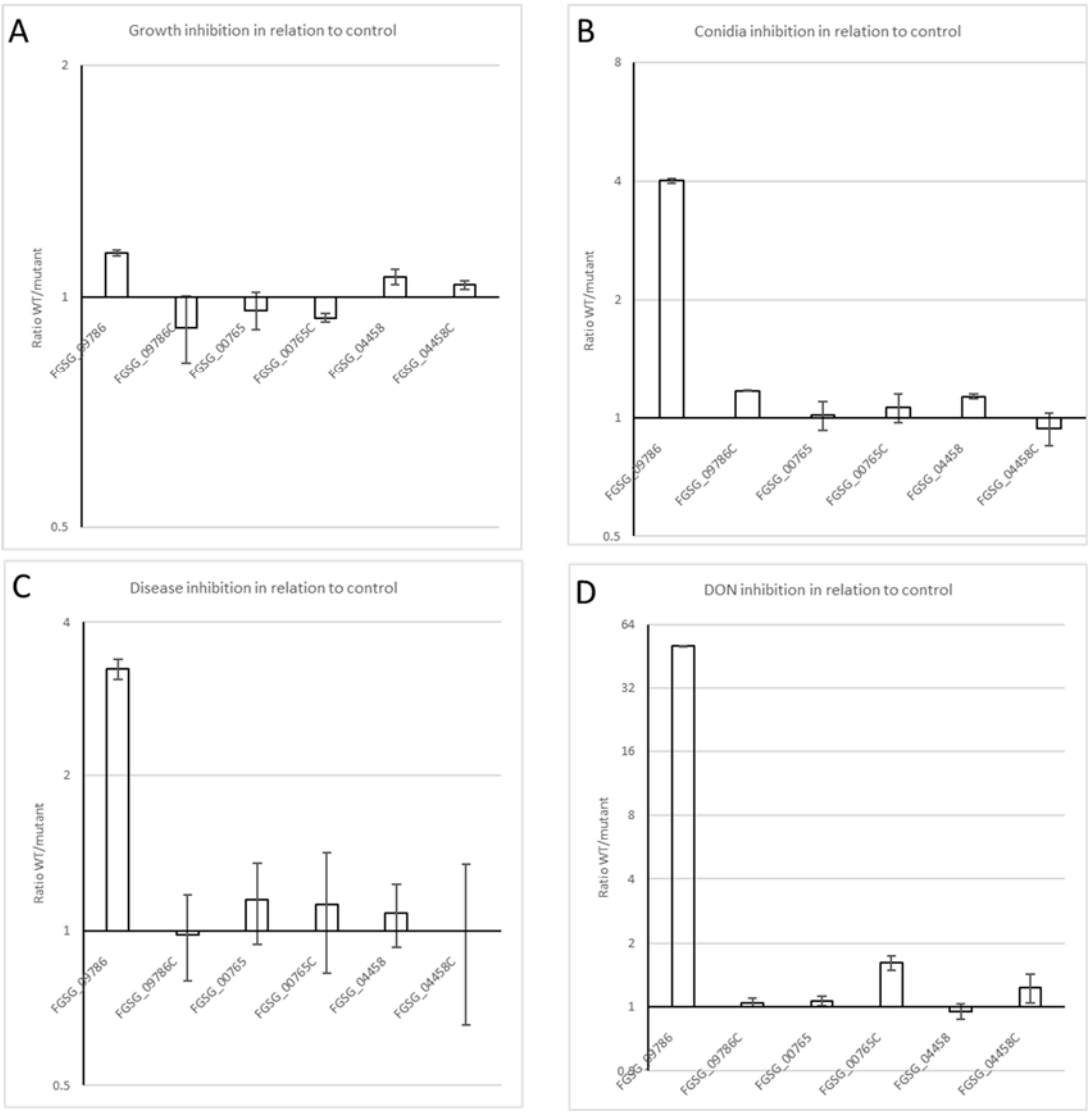

1119

1120 **Figure 6.** Phenotypic characterization of the mutants. Inhibition effect of deletions and complementations (C)
1121 compared with intact PH1 WT genes. Y=(PH1/Mutant or complement). FGSG_09786=*ΔFgNCP$_{NO}$,*
1122 FGSG_00765= *ΔFgNOD1* and FGSG_04458=*ΔFgNOD2.* (A) Colony diameter on CM agar. (B) Inhibition of conidiation.
1123 (C) Disease inhibition. (D) Inhibition of plant mycotoxin formation DON. Radial growth was little affected but conidia
1124 and diseases disease and especially the formation of DON was severely inhibited by deleting FGSG_09786. The
1125 deletion of the other genes showd no or little inhibition. Three replicates were used, and error bars show 95%
1126 confidence intervals for the mean values. Thus, the P-value for the null hypothesis for the same average for bars with
1127 non-overlapping error bars <<0.05.

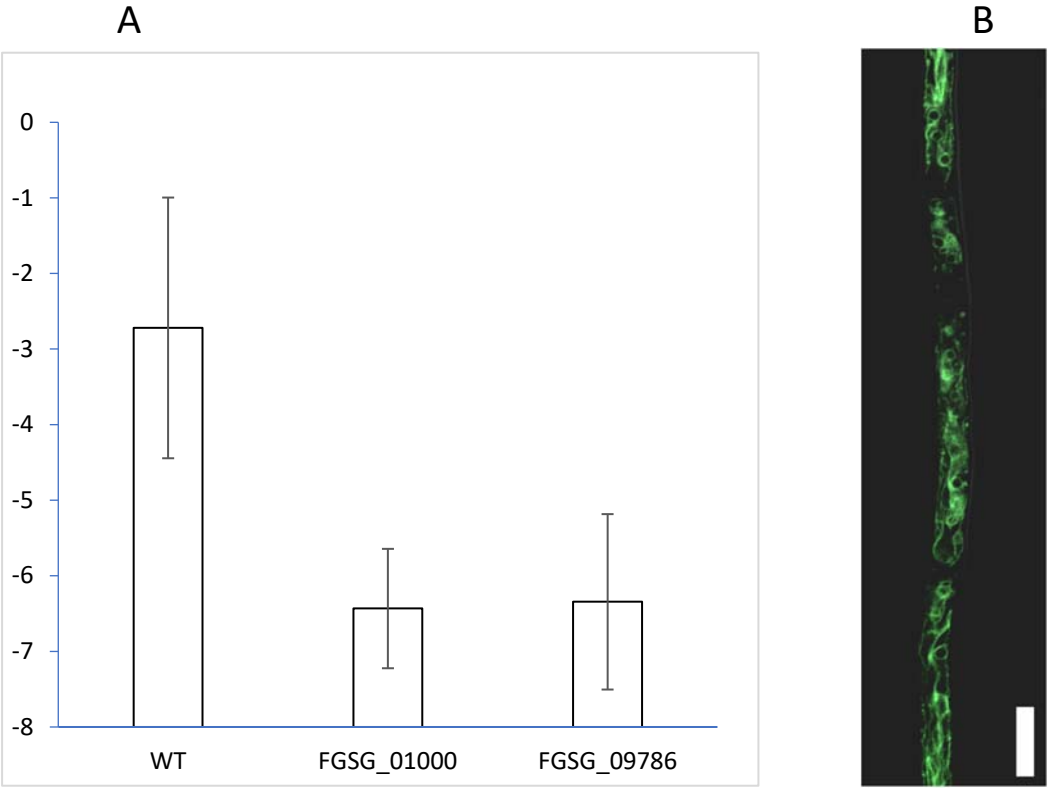

Figure 7. NO production in the FGSG_01000=*ΔFgCYP*$_{NO}$ mutant. *ΔFgCYP*$_{NO}$ mutant compared to WT (PH-1) and the FGSG_09786 as response to added bacteria free washings (containing bacterial MAMPs). (**A**) NO production was measured as LOG2 (NO signal/biomass signal) using confocal microscopy of large areas with many hyphae in WT=PH1, FGSG_01000= *ΔFgCYP*$_{NO}$ FGSG_09786= *ΔFgNCP*$_{NO}$ deletions and WT for NO formation rate (see methods). The FGSG_09786 was used as negative control for NO responses. Three replicates were used, and error bars show 95% confidence intervals for the mean values. Thus, the P-value for the null hypothesis for the same average of bars with non-overlapping error bars <<0.05. (**B**) FgCYP$_{NO}$-GFP (FGSG_01000-GFP) localizes to ER-like structures. Size bar 10μm. The results indicate that FGSG-01000 encodes FgCYP$_{NO}$ that receives electrons from FgNCP$_{NO}$ and produces NO.

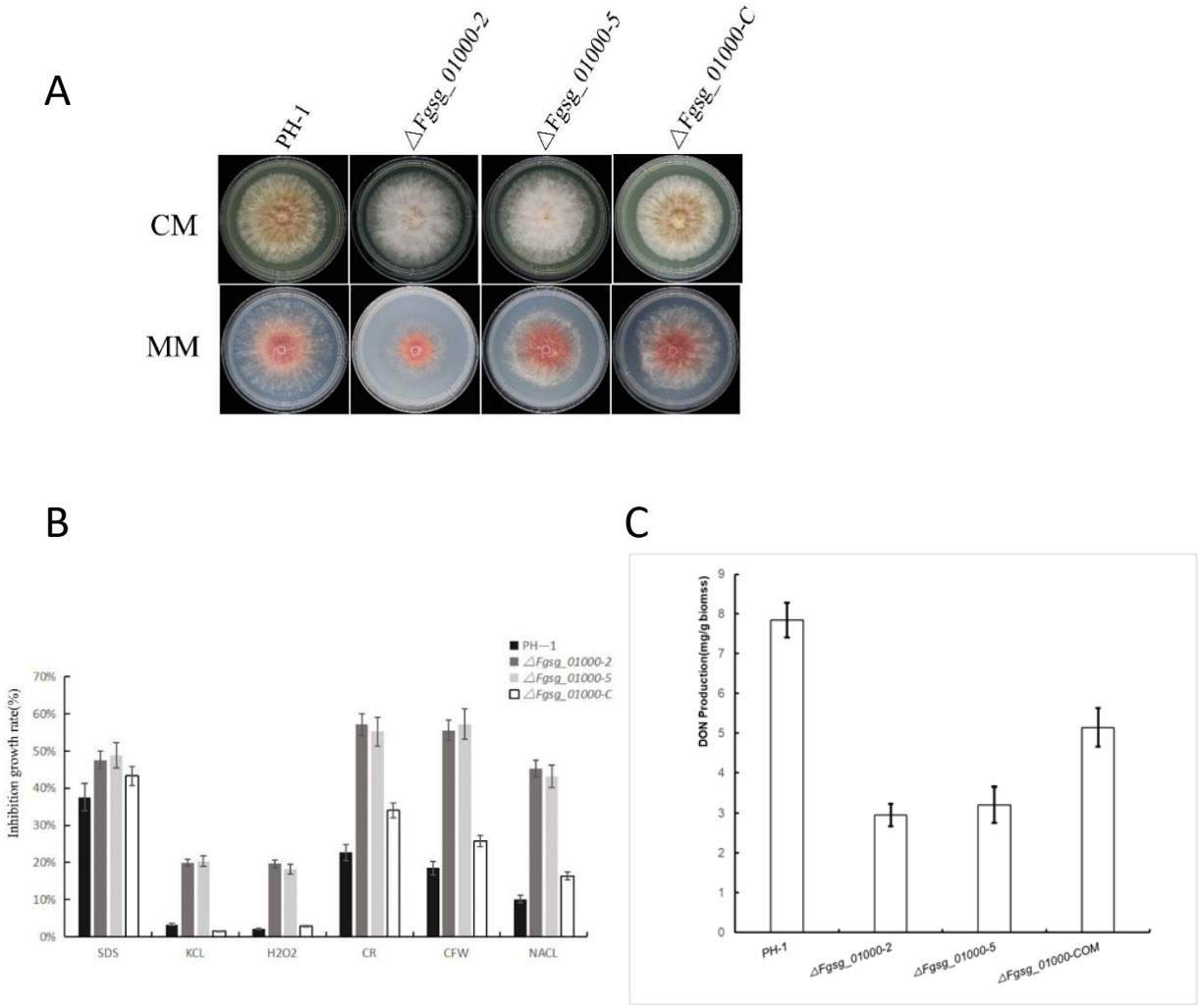

Figure 8. Phenotypic characterization of the *ΔFgCYP$_{NO}$* mutant strains Fgsg_01000-2 and Fgsg_01000-5. (**A)** Growth of WT (PH-1), mutants and complement strains on complete medium (CM) and minimal medium (MM). (**B**) Phenotypic effects of stress treatments by addition of stressors to CM-medium. SDS=0.01%, KCL=1M, H_2O_2=5 mM, Congo red CR=1 mg/ml, CFW=200μl/ml, NaCl=1M. Three replicates were used, and error bars show 95% confidence intervals for the mean values. Thus, the P-value for the null hypothesis for the same average of bars with non-overlapping error bars <<0.05. (**C**) Effect of FGSG_01000= *ΔFgCYP$_{NO}$* on DON mycotoxin production. There was little effect on growth caused by the deletion but more effects on stress phenotypes linked to cell membrane and cell wall effects as well as a pronounced effect on DON mycotoxin production. Three replicates were used, and error bars show 95% confidence intervals for the mean values. Thus, the P-value for the null hypothesis for the same average of bars with non-overlapping error bars <<0.05.

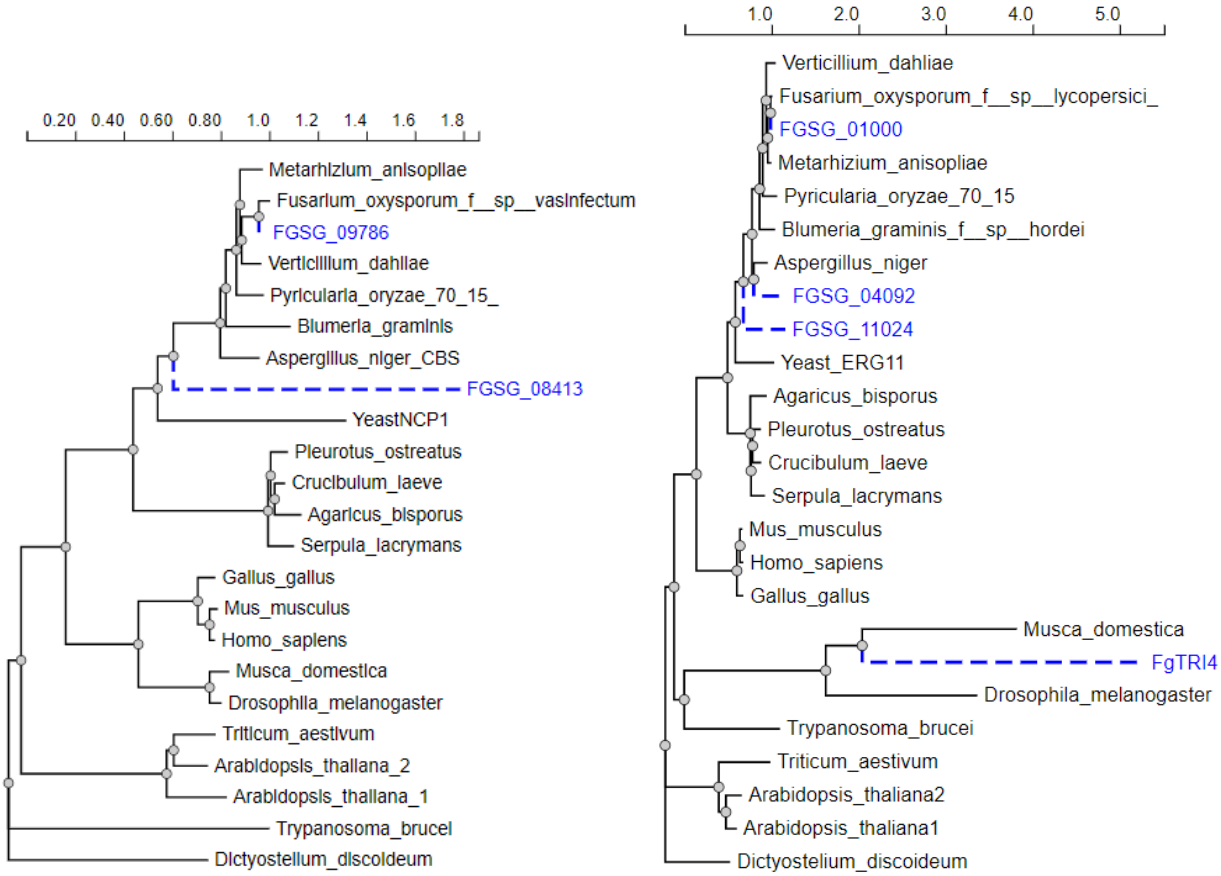

Figure 9. Comparing othologues of the two proteins (FGSG_09786 and FGSG_01000) involved in NO production in orthologous proteins from other eucaryotes at progressively larger taxonomic distance . (A) All proteins are annotated as NADPH-cytochrome-P450 oxidoreductases (NCPs) in the NIH database, and some are known to be involved in sterol synthesis. (B) All are CYPs in the database, and except FgTRI4 involved in DON synthesis, all are annotated as lanosterol 14-alpha-demethylases (=ERG11 in yeast) involved in converting lanosterol to the next step in sterol synthesis. The FGSG_04092 and FGSG_11024 only become activated late during infection, where Tri4 is highly activated *in planta* according to transcriptome data (not shown). For a complete analysis and protein sequences, see **Supplementary files SF7 and SF8**. Our analysis indicate that there are putative orthologues of the two NO generating proteins in all included species from amoeba to human and can also be involved in sterol synthesis.

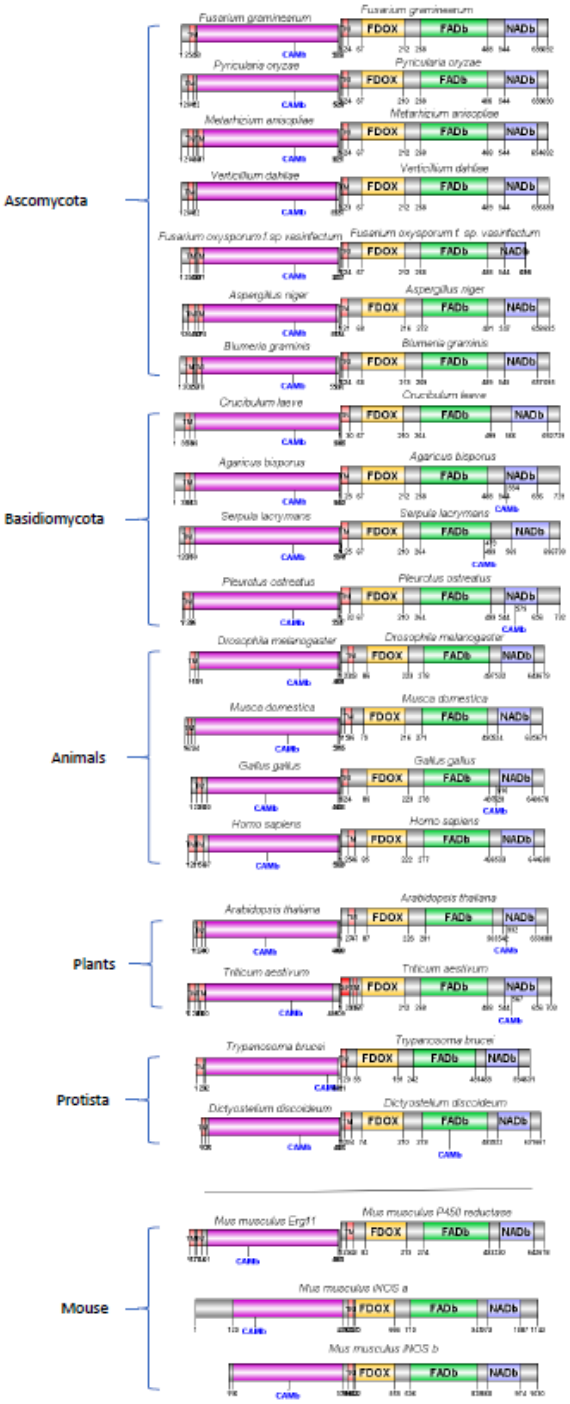

Figure 10. Domain structure of mouse iNOS (bottom) compared to the homologues to the CYP-part of the iNOS left of the hydrophobic helix (TM-marked) region and the heme-reductase part (NCP) to the right according to HMMER**.** The NCP Erg11 involved in ergosterol synthesis is the protein most like the $FgCYP_{NO}$ (FGSG_01000), and a P450 mouse reductase (NCP) is similar to the $FgNCP_{NO}$ involved in NO production. All these pairs except the iNOses have N-terminal TM regions predicted to be associated and inserted in the ER membrane by DeepLoc. All CYP-like proteins are predicted to be strongly Cam binding, and a few of the NCPs to the right are also predicted to be strongly CaM-binding. The rest of the NCPs are predicted to have cam-binding sites but are predicted to themselves be Cam-binding to a lesser degree (under the confident threshold level 1 [50] but might still have Cam binding possibility. For the complete analysis and protein sequences, see **Supplementary file SF6**. Our analysis show a remarkable similarity in domain structure and even distance between domains of the orthologous CYP-NCP pairs with the mouse iNOS. All CYP-NCP proteins contains the N-teminal part that is predicted to be an ER-anchor.

1201

1202 A

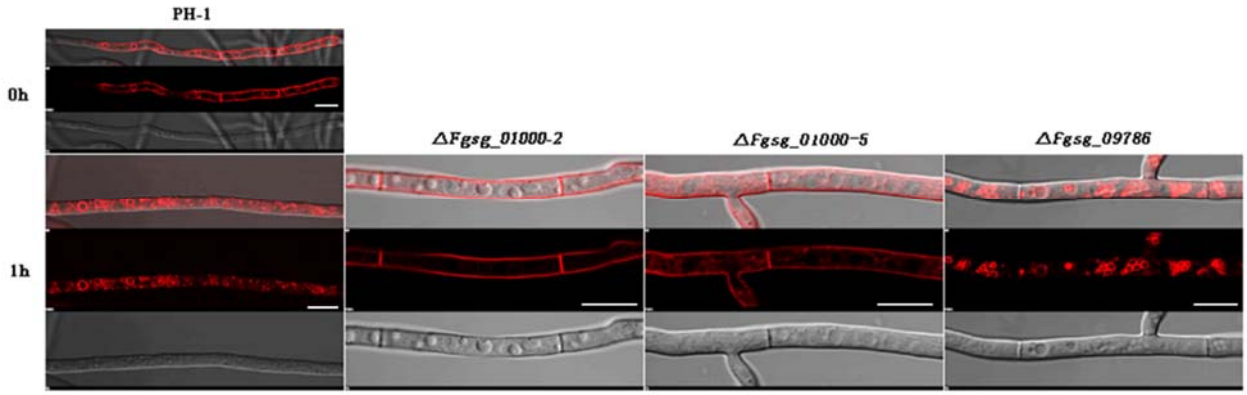

1203
1204

1205 B

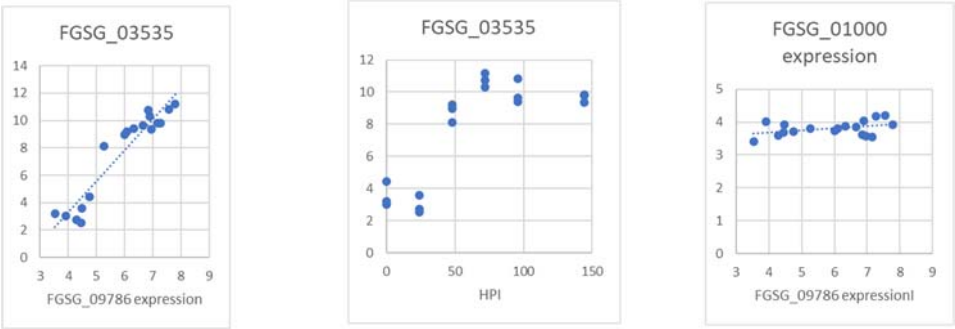

1206

1207 C

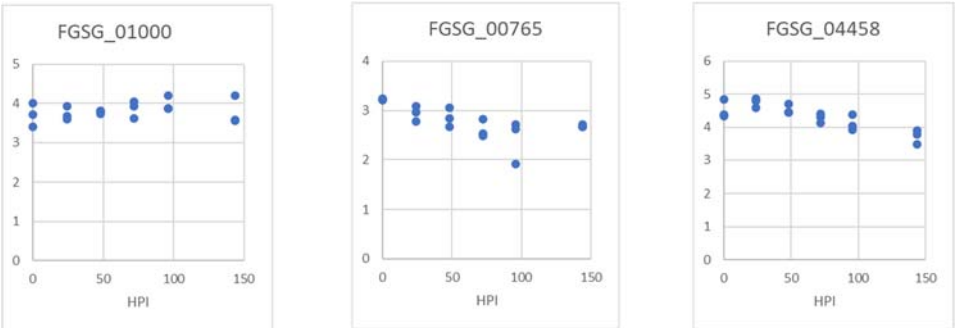

1208

1209 D E F

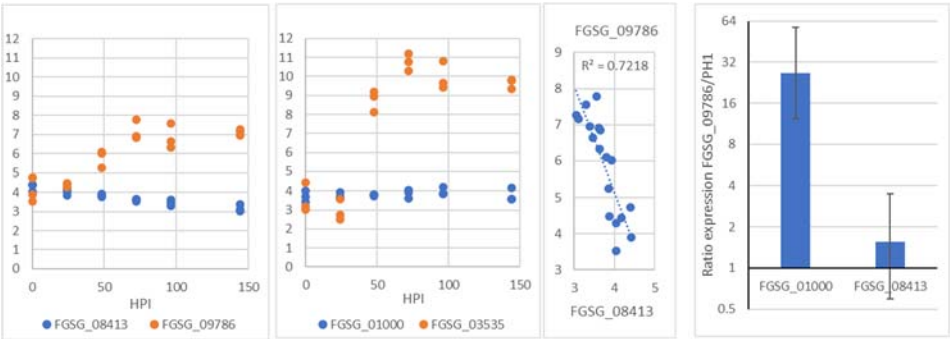

1210

1211 **Figure 11.** Effect of the *ΔFgCYP*$_{NO,ERG}$ on ergosterol biosynthesis and compensatory regulations when the NCP$_{NO,TRI,ERG}$
1212 is used to transfer electrons to the TRI4 heme protein (FGSG_FGSG_03535. (**A**) Staining endocytosis uptake using the
1213 endocytosis probe FM4-64 for 1h. Wt =PH1 takes up the stain by endocytosis, and the stain accumulates at the ER

around the nucleus. *ΔFgCYP*$_{NO,ERG}$ (FGSG_01000) is completely blocked for endocytosis, and the stain stays at the plasma membrane in normal-looking hyphae, and FGSG *ΔFgNCP*$_{NO,TRI,ERG}$ (FGSG_09786) is not severely blocked in endocytosis. DIC image to show that FGSG_01000 appears normal in intracellular structures. Size bars 10μm. (**B-E**) Co-regulation and expression during the course of infection of the two NO-producing genes compared with the primary DON-producing genes in a large transcriptome dataset with transcription during plant infection (Experiment FG1 with 3 replicates for each of 6 timepoints and a total N=18) from a previous study [54]. Expression axes are log2 expressions, and each dot represents data for the genes from one transcriptome. (**B**) Correlation between DON producing *FgCYP*$_{TRI}$ (FGSG_03535, Tri4) and *FgNCP*$_{NO,TRI,ERG}$ (FGSG_09786)(left). Expression of *FgCYP*$_{TRI}$ during the course of infection 0-144 hours post-infection (HPI) (middle). Correlation between DON producing *FgCYP*$_{TRI}$ (FGSG_03535, Tri4) and *FgCYP*$_{NO,TRI,ERG}$ (FGSG_09786)(right). (**C**) Expression of *FgCYP*$_{NO,ERG}$ (*FgNOD1* and *FgNOD2* 0-144 HPI showing NO upregulation of the genes linked to NO-production. (**D-E**) Regulation of *FgNCP*$_{NO,TRI,ERG}$ (FGSG_09786) compared to *FgNCP*$_{ERG}$ (FGSG_08413) and *FgCYP*$_{TRI}$ (FGSG_03535) and *FgCYP*$_{NO,ERG}$ (FGSG_01000) during the course of infection. (D) Expression of *FgNCP*$_{NO,TRI,ERG}$ increases during the course of infection (Left) as do *FgCYP*$_{TRI}$ right) while *FgNCP*$_{ERG}$ slightly decreases (left) and *FgCYP*$_{NO,ERG}$ does not change (right). (**E**) The negative correlation between FgNCP$_{NO,TRI}$ and FgNCP$_{ERG}$. (**F**) RT-qPCR test if *FgCYP*$_{NO,ERG}$ (FGSG_01000) and *FgNCP*$_{ERG}$ (FGSG_08413) are compensatory upregulated to aid ergosterol synthesis in the *ΔFgNCP*$_{NO,TRI,ERG}$ (FGSG_09786). Y-axis represents the ratio of expression of the respective genes in the *FgNCP*$_{NO,TRI,ERG}$ (FGSG_09786) mutant compared to the WT (PH1). Both genes potentially involved in ergosterol synthesis are upregulated, explaining why ergosterol-dependent endocytosis was expected in the *ΔFgNCP*$_{NO,TRI,ERG}$. Three replicates were used, and error bars show 95% confidence intervals for the mean values. Thus, the P-value for the null hypothesis for the same average with non-overlapping error bars <<0.05.

1236

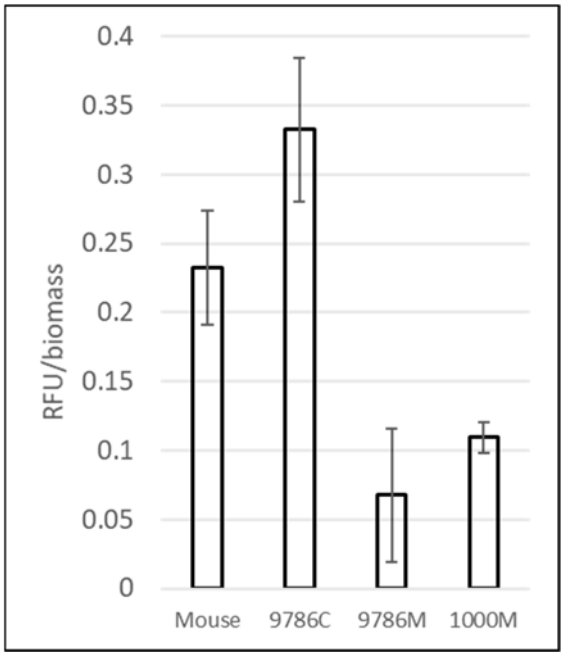

1237

1238 **Figure 12**. Complementing the *ΔNCP*$_{NO,TRI,ERG}$ (9786M) with the orthologue gene from mouse (Mouse) restores NO
1239 production to levels similar to the NCP$_{NO,TRI,ERG}$ complemented by the native gene (9786C). The *ΔNCP*$_{NO,TRI,ERG}$ (9786M)
1240 and the *ΔCYP*$_{NO,ERG}$ (1000M) were used as negative controls. Three replicates were used, and error bars show 95%
1241 confidence intervals for the mean values. Thus, the P-value for the null hypothesis for the same average of bars with
1242 non-overlapping error bars <<0.05.

1243

1244 A

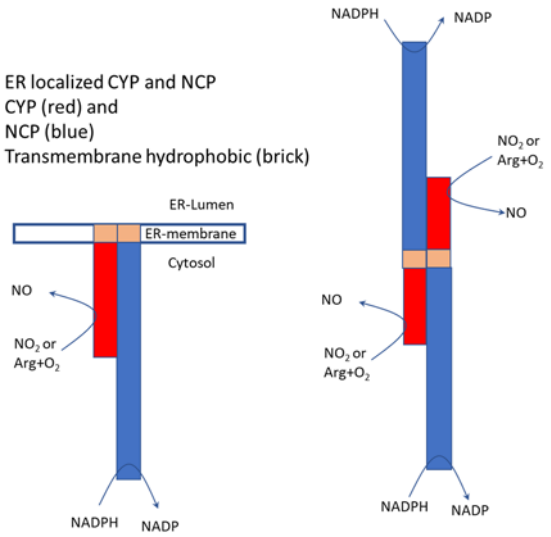

1245

1246 B

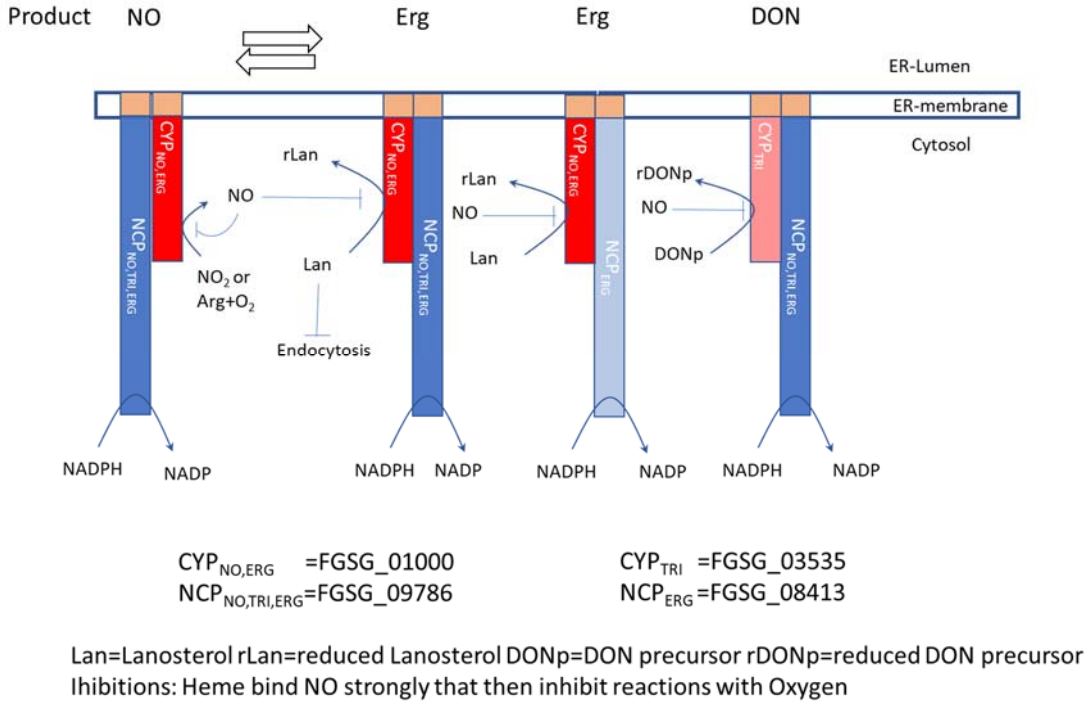

1247

1248 **Figure 13.** Conceptual models. (**A**) Model for the arrangement of domains in the ER-localized CYP_{NO} and
1249 NCP_{NO} implied in this study compared with the localization of domains in a NOS-dimer [8]. (**B**) A conceptual
1250 model for the dynamic arrangements and re-arrangements of the CYPs and NCPs at the ER membrane
1251 needed for NO, ergosterol and DON production. Note that interactions needed for electron transfer
1252 between proteins do not need physical contact, only brief closeness (100nm seems to be enough) [58,59,65,108].
1253 The relative abundance of the proteins and more shapes more favourable to electron transfers brought
1254 about by conformational changes due to Ca^{2+} binding to CAM binding sites (Fig. 10) could favour such
1255 interactions at a distance, making it very flexible and quick to change the products' proportions by gene
1256 expression and calcium signalling. The model, however, depicts the symbols for the proteins as if they

1257 need to be in direct contact. This study's main proteins, $FgCYP_{NO,ERG}$ and $FgNCP_{NO,TRI,ERG}$, appear to have 2,
1258 respective 3, functions in *F. graminearum*. NO binds to $FgCYP_{NO,ERG}$ heme, and self inhibits NO [9] and ergosterol
1259 formation at lanosterol [109] an effect known to reduce endocytosis[110,111], and $FgCYP_{TRI}$ since DON formation
1260 seems to be shut off by NO-donors [29].

1261

1262 **Table 1**. Conversion table of gene names

ORF id F. Graminearum paralogues	Suggested name based on 1 chemical property and 2 cellular functions	Previously assigned chemical function	Names used in F. graminearum and (other filamentous)	Saccaromyces cereviseae	Mammals
FGSG_01000[1]	*FgCYP(NO,ERG)*	C14-α-demetylase	*Fgcyp51B*[2]	*Erg11*	*cyp51*
FGSG_04092[1]	-	C14-α-demetylase	*Fgcyp51A*[2]	-	-
FGSG_11024[1]	-	C14-α-demetylase	*FgCyp 51C*[2] *(uniquefor Fg)*	-	-
FGSG_03535	*FgCYP(TRI)*	trichodiene oxygenase	*FgTri4*[3]	-	-
FGSG_09786[1]	*FgNCP(NO,TRI,ERG)*	NADPH-cytochrome P450 reductase	*FgCPR*[4]	YeastNCP1	*P450R*
FGSG_08413[1]	*FgNCP(ERG)*	NADPH-cytochrome P450 reductase	-		

1263

1264 1. According to this study
1265 2. References [73,112]
1266 3. Reference [113]
1267 4. Reference [67]

1268

Supplementary material

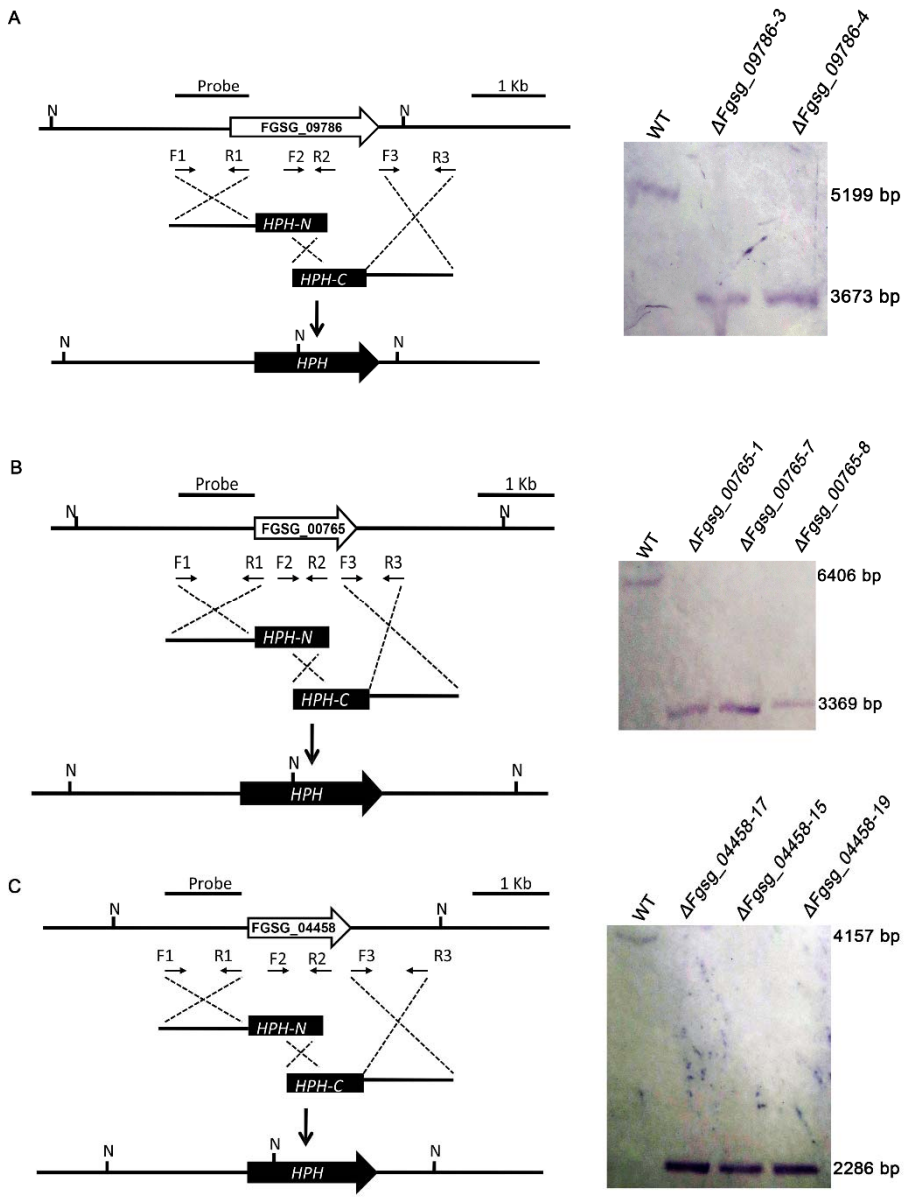

Figure S1 Targeted gene-replacement construct and Southern blot assays. Each targeted gene-replacement construct is shown in the left panel. The primer pairs F1 and R1, F3 and R3 were used to generate the gene replacement constructs. Primers F2 and R2 were used for mutant screening and identification. (A) Targeted deletion of FGSG_09786. Nde I-digested genomic DNAs showed a 5.20 kb band in the WT and a 3.67 kb band in the mutants. (B) Targeted deletion of FGSG_00765. Nde I-digested genomic DNAs showed a 6.41 kb band in the WT and a 3.37 kb band in the mutants. (C) Targeted gene deletion of FGSG_04458. Nde I-digested genomic DNAs showed a 4.16 kb band in the WT and a 2.29 kb band in the mutants.

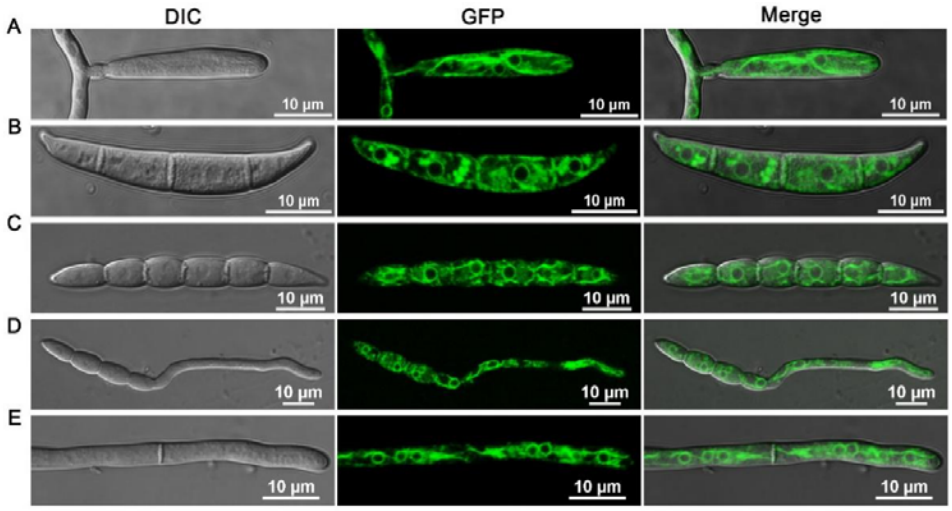

II

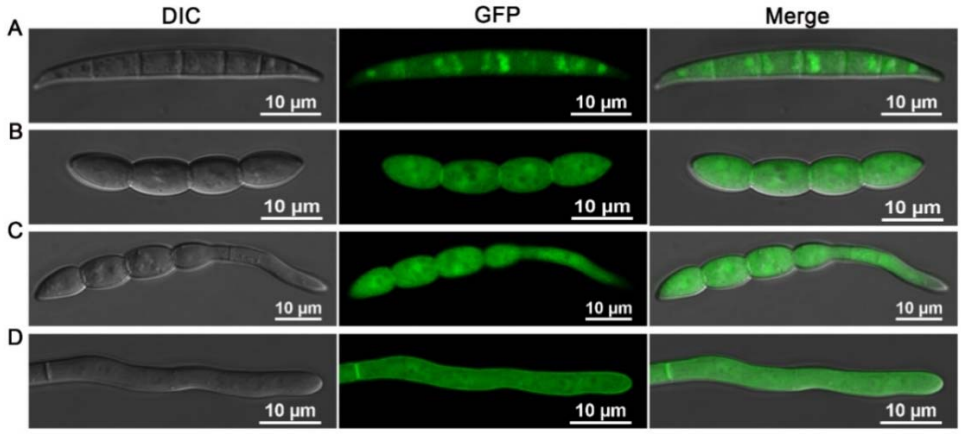

III

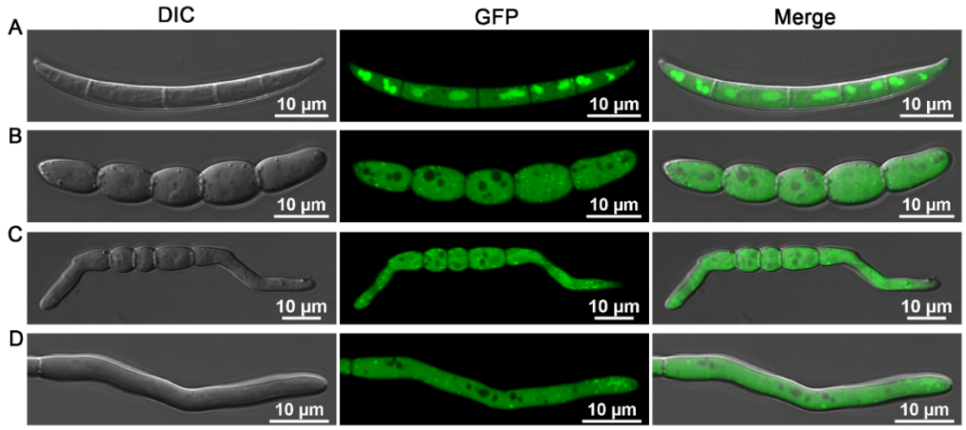

Figure S2 Localization of complements labelled with GFP. (I) $FgNCP_{NO}$ (FGSG_09786) localizes to ER like structures. (II) FgNOD1 (FGSG_00765) principally localizes to the cytoplasm. It also is observed at the septum between cellular compartments in growing hypha. (III) FgNOD2 (FGSG_04458) localizes to the cytoplasm and small dot-like structures in hyphae and germinated conidia. The clustered fluorescence in conidia from FgNOD1 and FgNOD2 mutants may be GFP proteins undergoing degradation at the vacuoles. (A) Conidia (B) Conidia just before germination (C) Germinated conidia (D) Hyphae.

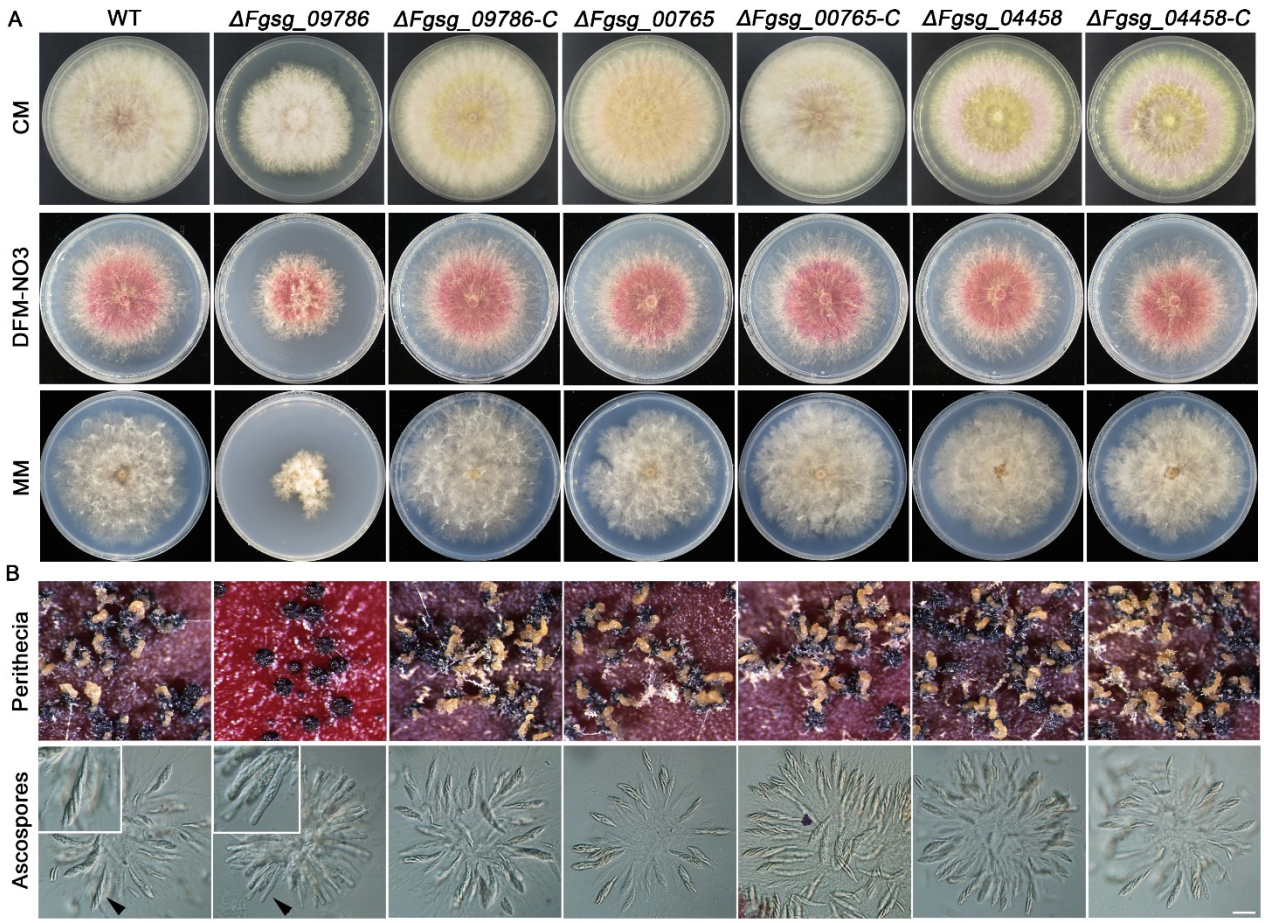

Figure S3 (A) Growth of WT (PH-1), mutant and complementation strains on CM, DFM-NO_3 containing NO_3 as sole nitrogen source and MM medium. $FgNCP_{NO}$ (FGSG_09786) is required for the hyphal growth in CM, DFM-NO3 and MM medium. (B) Sexual reproduction of WT, mutants and complementation strains. $FgNCP_{NO}$ (FGSG_09786) is essential for forming normal ascospores and their ejection from the perithecia (yellow masses). The black arrowhead indicates ascus zoomed in and shown in the top left corner showing a changed morphology of asci. It is mainly the deletion of FGSG_09786 that show phenotypic colony effects and effects on sexual spore formation

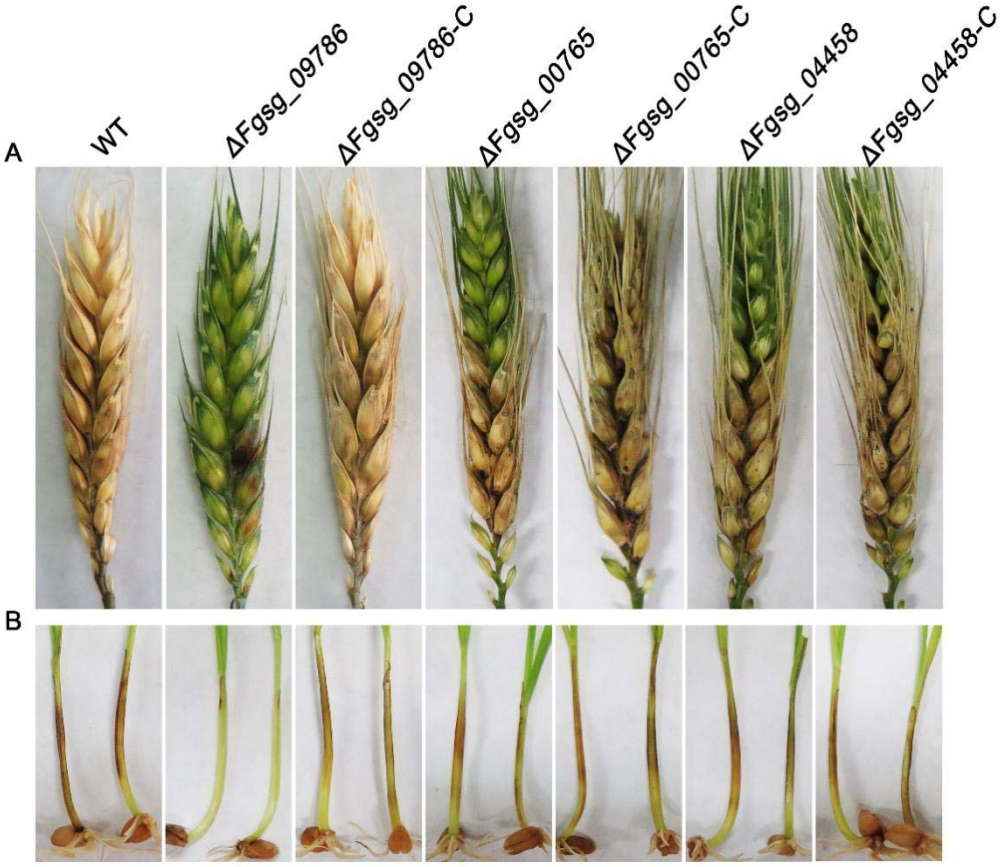

Figure S4. Pathogenicity of each strain on (A) Wheat heads and (B) seedlings. *ΔFgsg_09786* showed reduced virulence in both assays. Loss of chlorophyll green colour and browning lesions indicate infection. The FGSG_09786 has completely lost the ability to spread in the tissue, while the other NOD mutant strains were similar to their respective complement strains.

1312

1313 **Table S5**. PSORTII predicted localization output for the ER-membrane localized $FgNCP_{NO}$

1314 *k* = 9/23

1315 34.8 %: nuclear

1316 21.7 %: mitochondrial

1317 21.7 %: cytoplasmic

1318 8.7 %: vesicles of secretory system

1319 4.3 %: endoplasmic reticulum

1320 4.3 %: peroxisomal

1321 4.3 %: vacuolar

1322 prediction for 15761259072134 is nuc (k=23)

1323

1324

1325

1326

1327

1328

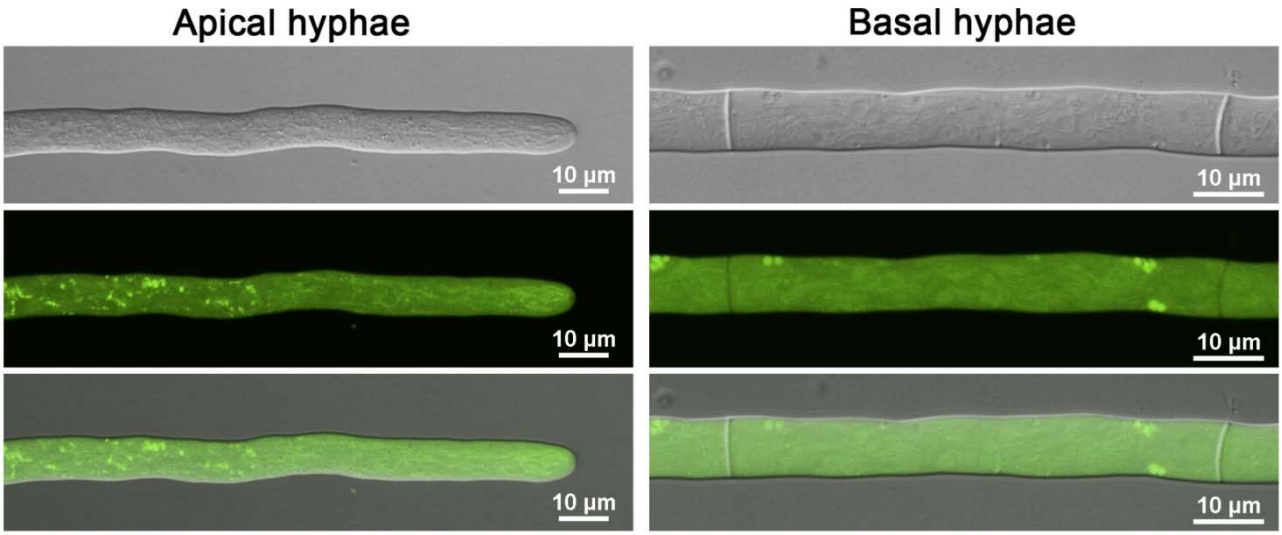

1329

1330 **Figure S6**. Localization of a potential $FgCYP_{NO}$ (FGSG_07925) labelled with GFP. Localization is not to ER as
1331 expected, so this is not the $FgCYP_{NO}$. (Top) DIC images (Middle) GFP images (Bottom) Merge.

1332

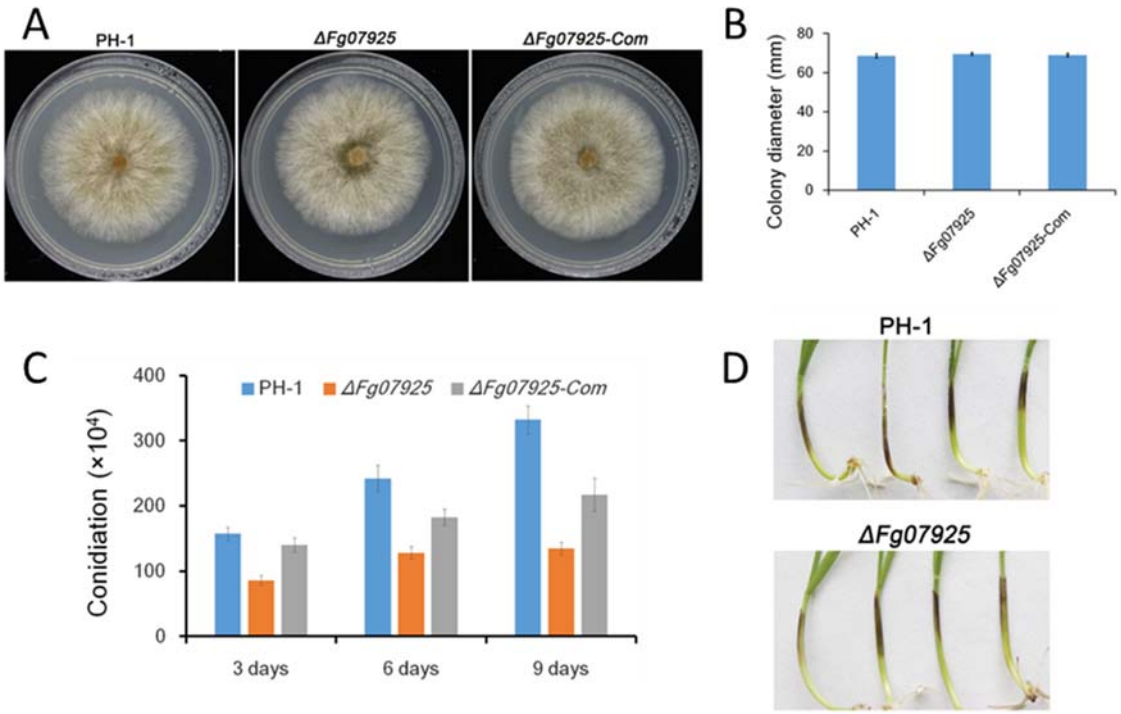

Figure S7. Phenotypic characterization of a CYP gene deletion mutant (FGSG_07925), although this gene cannot encode for the CYP_{NO} since it is not ER-localized (A and B). Deletion of FGSG_07925 does not affect fungal growth on a CM medium. (C) FGSG_07925 appear to be required for conidiation. (D) Deletion of FGSG_07925 does not either affect fungal pathogenicity on wheat coleoptiles. In B and C error bars are SEM and N=3

Table S8. List of genes encoding for predicted heme-containing proteins (*FgCYP$_{NO}$*) sorted after gene expression most correlated with *FgNCP$_{NO}$* expression (FGSG_09786) as target gene (T). We first tried to knock out and localize FGSG_07925, but that was not localized to the ER as FGSG_09786. As shown in the table, FGSG_01000 is the most likely *FgCYP$_{NO}$* taking all the following 5 criteria into account since it is (1) a predicted heme-containing protein that is not a predicted NOD. (2) It is transcriptionally highly correlated with *FgNCP$_{NO}$* expression in the dataset from short-term responses to purified bacterial MAMPs. (3) It is predicted to localize to the ER membrane where the FgCYP$_{NO}$ can be found. (4) The maximum expression of the FGSG_01000 is of the same magnitude as the *FgNCP$_{NO}$* expression, which would be expected if they work together as a heterodimer to make NO (5) similar to the homo-dimer iNOS assembly.

id	Corr	MAX/MaxT*	Annot/location (ER),predictor,experimental/comment
FGSG_09786	1	1	HemeR/located to ER, DeepLoc, Our data
FGSG_07925	0.786385	14.42007	Heme/Not in ER, DeepLoc, Our data
FGSG_00765	0.767517	2.010113	NOD1/Not in ER, DeepLoc, Our data/removes NO toxicity
FGSG_04458	0.517216	5.949739	NOD2/Not in ER, DeepLoc, Our data/removes NO toxicity
FGSG_01000	0.516057	1.00908	Heme/ER-membrane, DeepLoc/GOOD CANDIDATE
FGSG_09373	0.425022	5.08457	Heme/Not in ER, Deeploc
FGSG_01972	0.295199	0.264709	Heme/Not in ER, Deeploc
FGSG_10305	0.286719	2.102463	Heme/Not in ER, Deeploc
FGSG_10881	0.269646	6.574407	Heme/Not in ER, Deeploc
FGSG_11195	0.247331	0.008291	Heme/Not in ER, Deeploc
FGSG_02982	0.237979	0.019898	Heme/Heme pred. to ER, Deeploc/Expression too low
FGSG_07977	0.237186	0.000886	Heme/Not in ER, Deeploc
FGSG_12534	0.234465	0.185611	Heme/Heme pred. to ER, Deeploc/Expression too low

*MAX expression of gene/ Max expression of Target gene (FGSG_09786).

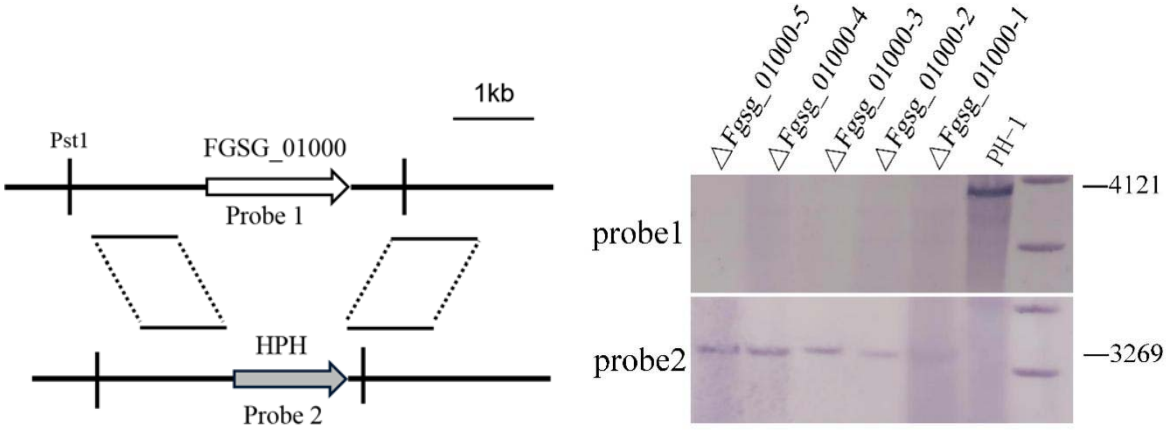

Figure S9 Targeted gene-replacement construct and Southern blot assays for the deletion of FGSG_01000. The targeted gene-replacement construct is shown (left panel), and a Southern blot of digested genomic DNAs showed a 4.12 kb band in the WT and a predicted 3.27 kb band in the deletion mutants.

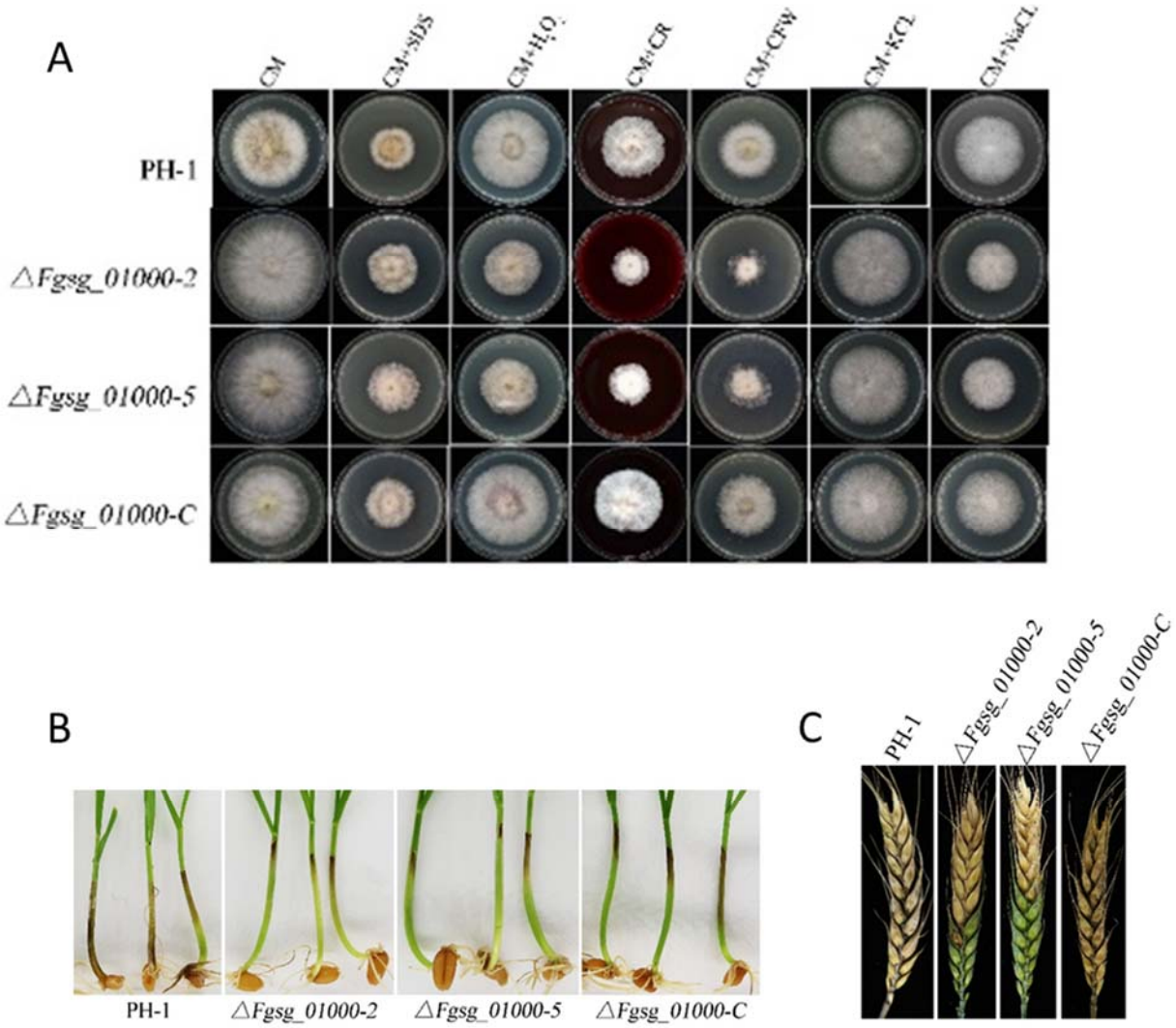

Figure S10. Phenotypic effects of the FGSG_01000 deletion (A) Effect of stress treatment by adding stressors to CM-medium WT (PH-1), mutant strains and complement strain. SDS=0.01%, H_2O_2=5 mM, Congo red CR=1 mg/ml, CFW=200μl/ml, KCL=1M, NaCl=1M. (B) Effect deletion and complementation on wheat seedling infection and (C) wheat head infection. As for the deletion of FGSG_09786 (the NCP taking part in making NO), the stress treatments affecting the integrity of the cell wall and cell membrane are most affected, as well as infection of both wheat seedlings and wheat heads.

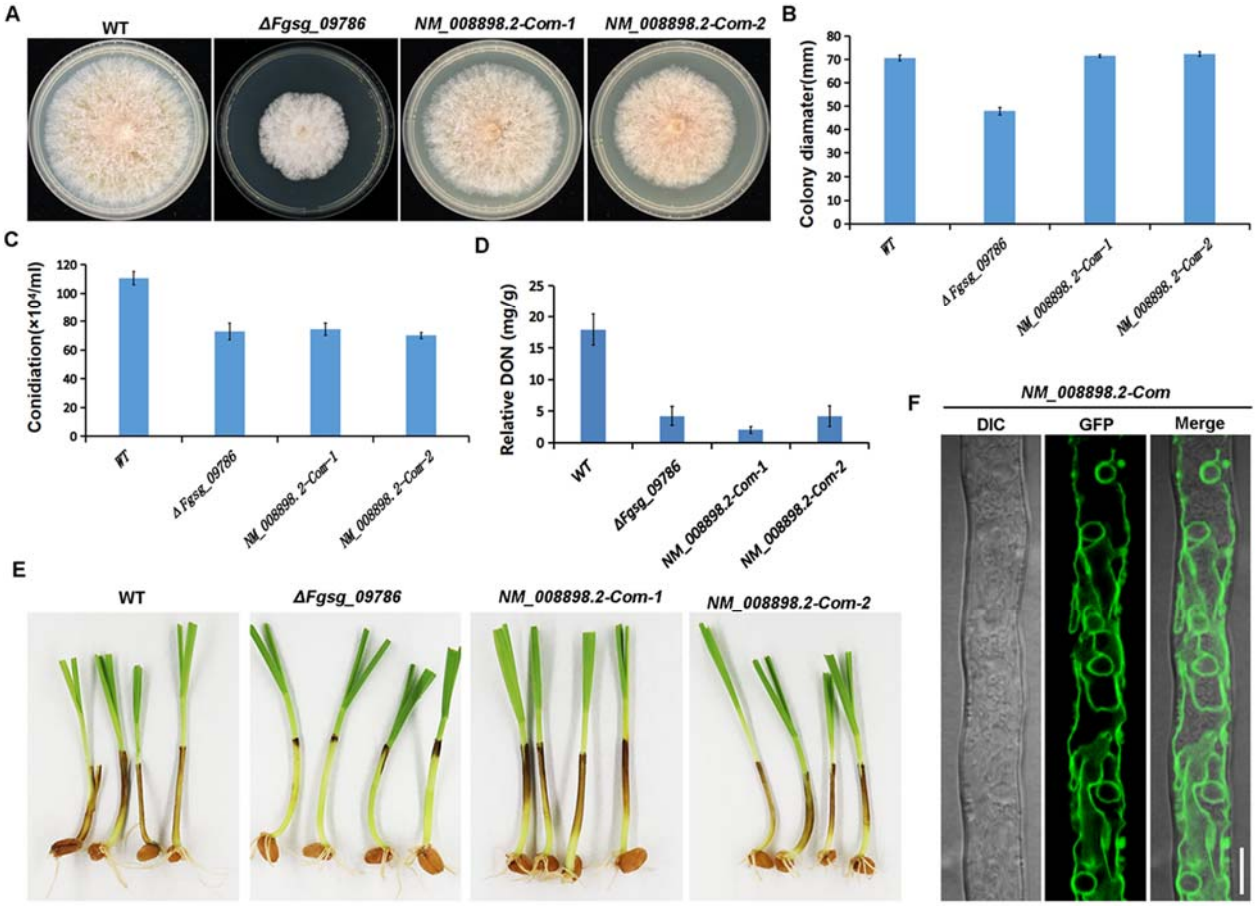

Figure S11 Complementation of the $NCP_{NO,TRI,ERG}$ deletion with the orthologous gene from mouse NM_008898. Effect on colony morphology (A), colony growth (B), conidiation (C), DON production (D) and pathogenicity (E). The mouse gene used for complementation was tagged with GFP and showed typical ER localization (F) (sizebar 10µm). The deleted $NCP_{NO,TRI,ERG}$ showed similar phenotypes as the WT (PH-1) except for conidiation and for DON-production, showing that the mouse gene cannot completely complement all functions. In B-D error bars are SEM and N=3.

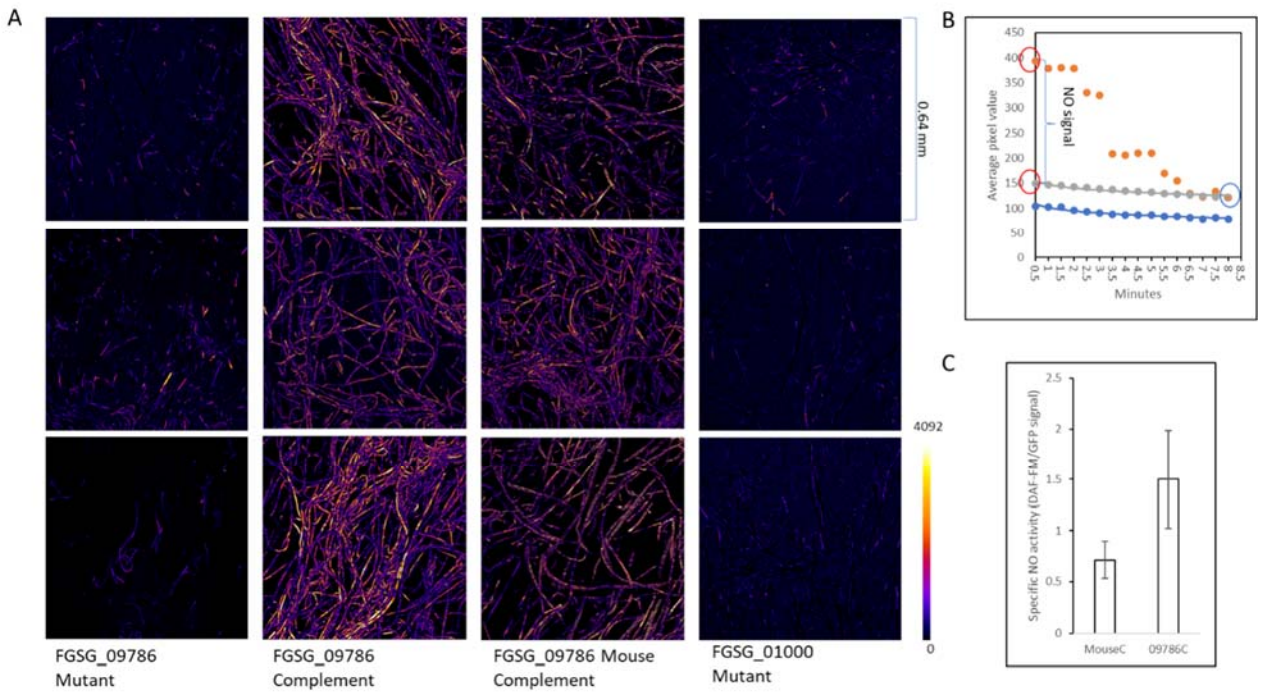

1382

1383 **Figure S12**. NO formation by the $FgNCP_{NO,TRI,ERG}$ mutant (ΔFGSG_09786), complementation with the native gene
1384 complement (FGSG_09586-GFP, FgNCP-GFP) encoding the native NCP protein, and the complementation with a
1385 mouse orthologous gene (Mouse-GFP) encoding the mouse NCP protein. The mutant of the NO forming gene for the
1386 $CYP_{NO,ERG}$ (FGSG_01000) the $NCP_{NO,TRI,ERG}$ delivers electrons to and makes NO was used as an extra negative control.
1387 All images have been handled in the same way. NO forms immediately in DAF FM DA solution (0.5 minutes) and then
1388 bleaches under the blue light laser. Both the fluorescent NO derivative of DAF-FM and the GFP-fusion complement
1389 fluorescence green excited by the blue laser. However, the stronger DAF-FM NO signal fades quickly, and the fading
1390 of the GFP signal is much slower and very reproducible. Thus, the 0.5-minute signal from the NO can be reconstructed
1391 using the decay function or the GFP signal that decreases exponentially with a constant percentage per time unit. (**A**)
1392 The reconstructed 0.5-minute NO signal images are shown using a "fire" colour scale between 0-4092 (colour scale in
1393 the lower right corner). (**B**) Illustration of how the reconstruction was done. Blue curves show that the bleach signal
1394 of the GFP decreases with the same percentage for each time unit (like radioactive decay). The reconstructed grey
1395 curve is based on the end value (marked by a blue oval) where only GFP fluorescence is left using the blue curve as a
1396 reference for the loss of GFP fluorescence. The NO signal at 0.5 minutes equals the difference between the
1397 reconstructed 0.5-minute signal for the GFP and the 0.5 signal for GFP+NO. (**C)** Specific NO forming activity by the two
1398 complement proteins as DAF-FM signal/GFP signal. Three replicates were used, and error bars show 95% confidence
1399 intervals for the mean values. Thus, the P-value for the null hypothesis for the same average of bars with non-
1400 overlapping error bars <<0.05.

1401 The results show that the mouse NCP can successfully complement the deleted $FgNCP_{NO,TRI,ERG}$ for most NO
1402 formations. Note: We had to mount the fungus in an isotonic pH6-7 phosphate buffer for the GFP signal not to fade
1403 quickly. That indicates that blue light can compromise membrane permeability and lower cytosolic pH, leading to
1404 lower fluorescence as GFP fluorescence is pH sensitive.

1405

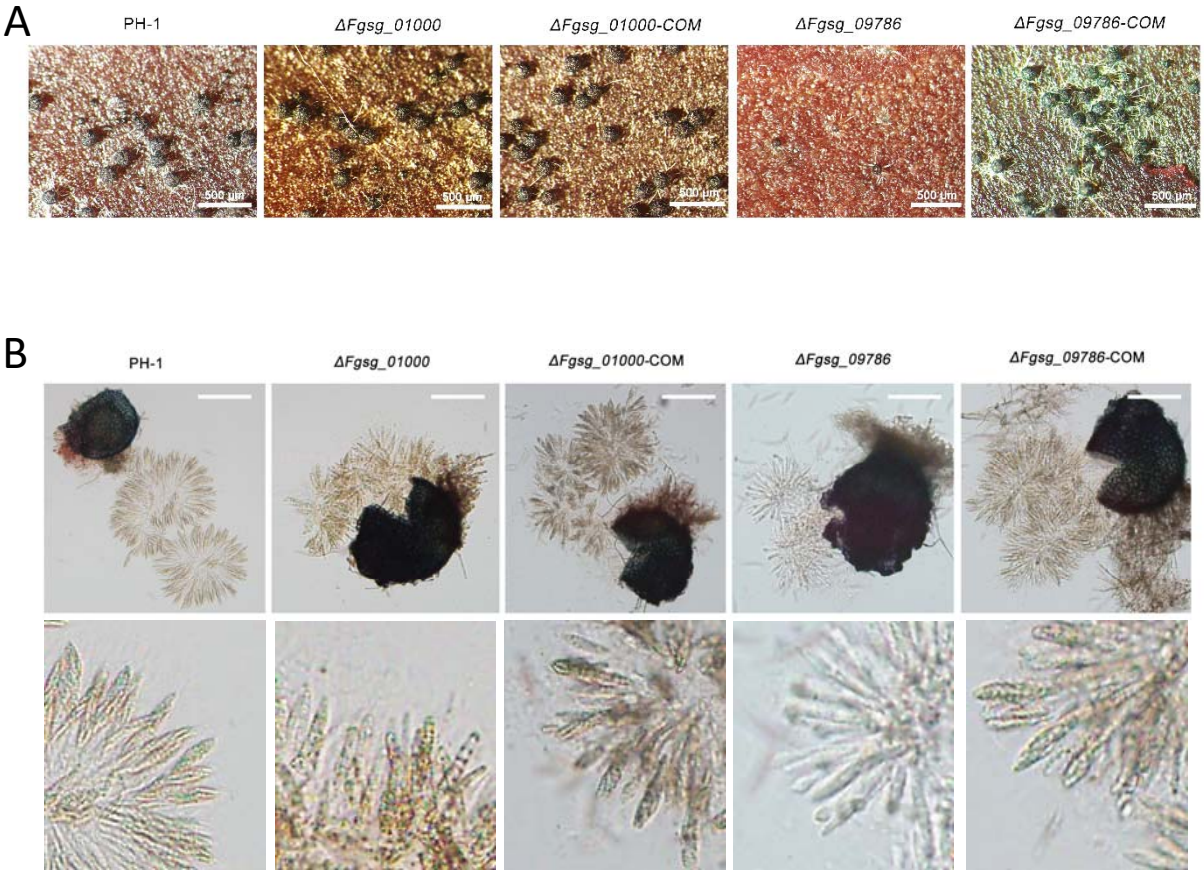

Figure S13. Perithecia formation and ascospore formation on carrot agar. (**A**) Perithecia (size bars 100 µm). Only Δ*Fgsg_09786* show a reduced number of perithecia. (**B**) Asci and ascospores (Size bars 50 µm). Both mutants show abnormal asci. Δ*Fgsg_01000* has septate asci that appear empty of spores. Also, Δ*Fgsg_09786* asci appear empty of normal-looking ascospores.

1412 **Table S14** Primers used in this study

Primers	Sequence (5'-3')	Application
FGSG01000AF	TAGGCTTTGGAATTTGGTTGAG	FGSG_01000's deletion and probe
FGSG01000AR	TTGACCTCCACTAGCTCCAGCCAAGCC GGTTGGGTGTTGTAAGGAGGA	
FGSG01000BF	GAATAGAGTAGATGCCGACCGCGGGTTCGAGCAAAAGCCA TCACATT	
FGSG01000BR	CCAACCCCTTCGCATCAG	
YG/F	GATGTAGGAGGGCGTGGATATGTCCT	
HYG/R	AACCCGCGGTCGGCATCTACTCTATTC	
HYG/F	GGCTTGGCTGGAGCTAGTGGAGGTCAA	
HY/R	GTATTGACCGATTCCTTGCGGTCCGAA	
FGSG01000OF	TACAGCCGCATTGAGTTG	Verification of *ΔFgsg01000*
FGSG01000OR	CATGGGAAGCAGTAAAGATAG	
FGSG01000UA	CATATTAAGCGGGGCATTAGAG	
H853	GACAGACGTCGCGGTGAGTT	
FGSG01000PF	AAGCACCATCACATACGG	Southern blot for *ΔFgsg01000* confirmation
FGSG01000PR	ATATCGGCAATGCCAGAC	
FGSG01000CF	agggaacaaaagctgggtaccCGATAAAGGGTTGATTCTG	Complementation of *ΔFgsg01000*
FGSG01000CR	gcccttgctcaccataagcttCTGGCGTCGCTCCCAGTGAATGT	
FGSG01000qRT-F	GTGCTACCGACTCTGCCTTC	qRT-PCR
FGSG01000qRT-R	AACCAGCCTGAGCTTCGATA	
FGSG08413qRT-F	AGCTGACGTCGGACTAGGAA	
FGSG08413qRT-R	GTGCTACCGACTCTGCCTTC	
FgbTubulin-qRT-F	GAGGGTATGGACGAGATGGAA	
FgbTubulin-qRT-R	GTCGGCGTCTTGGTATTGC	
FGSG09786AF	TCGGAATCCTCGTTTCAAGT	FGSG_09786's deletion and

FGSG09786AR	TTGACCTCCACTAGCTCCAGCCAAGCCAAGTATGCGACCGTTCCAAG	probe
FGSG09786BF	GAATAGAGTAGATGCCGACCGCGGGTTATGTATTCGGAGTAGACTTGGG	
FGSG09786BR	TGCGAGATGGCAGTTCAG	
FGSG09786OF	CCGCTATTACTCCATCTCCTCC	Verification of *ΔFgsg09786*
FGSG09786OR	GACTTACCTGCCATTCCTTCTC	
FGSG09786UA	GCAGCGTGGCTTATCGGTAT	
FGSG09786CF	agggaacaaaagctgggtaccAAGGAATAGGCGGTGTCAAGC	Complementation of *ΔFgsg09786*
FGSG09786CR	gcccttgctcaccataagcttTGACCAAACATCCTCCTGCG	
Mouse-09786-F	TCTAGCGGTCCAGTAGCCGTCATGGGGGACTCTCACGAAG	Complementation of *ΔFgsg09786* with mouse homologue
Mouse-09786-R	gcccttgctcaccataagcttGCTCCATACATCCAGCGAGTA	
FGSG_09786 promoter-F	agggaacaaaagctgggtaccAAGGAATAGGCGGTGTCAAGC	
FGSG_09786 promoter-R	GACGGCTACTGGACCGCTAGA	
FGSG00765AF	GAGTCAAGTTGGCTCTGTCA	FGSG_00765's deletion and probe
FGSG00765AR	TTGACCTCCACTAGCTCCAGCCAAGCCCGGTAGAAGATGGTGGTG	
FGSG00765BF	GAATAGAGTAGATGCCGACCGCGGGTTGTGCTACCTGCCCATTCTC	
FGSG00765BR	ATCCCGACTCCAAACTGC	
FGSG00765OF	CGTGCCCTTACCGCTGTT	Verification of *ΔFgsg00765*
FGSG00765OR	GGATTCGGCAAGGTGAGTCT	
FGSG00765UA	CATCAAGTGACCGTCGTGG	
FGSG00765CF	agggaacaaaagctgggtaccCATCAAGTGACCGTCGTGG	Complementation of *ΔFgsg00765*
FGSG00765CR	gcccttgctcaccataagcttTACCGCTGAGAATGGGCAG	

FGSG04458AF	TGCTGGGACTGTTCAACTAATG	FGSG_04458's deletion and probe
FGSG04458AR	TTGACCTCCACTAGCTCCAGCCAAGCCGCTGTTTGTCTATTG TGCCTGT	
FGSG04458BF	GAATAGAGTAGATGCCGACCGCGGGTTACAGCGAAAGCGT TATAGATTG	
FGSG04458BR	GTGGCGGGATTGATGAGA	
FGSG04458OF	CTCCGCAACCAACAAACAG	Verification of *ΔFgsg04458*
FGSG04458OR	GGGACCGCAGATGAAATACTC	
FGSG04458UA	CGCCGATGCCATTGAAGA	
FGSG04458CF	agggaacaaaagctgggtaccGGAGAAATGGAGTATGGAGGAC	Complementation of *ΔFgsg04458*
FGSG04458CR	gcccttgctcaccataagcttGACGTCGCCGGTCTTGAAGA	
FGSG07925AF	CAACATTGGGAACTGTAACCT	FGSG_07925's deletion and probe
FGSG07925AR	TTGACCTCCACTAGCTCCAGCCAAGCCAGTGATTGCTGTGG CTCTGA	
FGSG07925BF	GAATAGAGTAGATGCCGACCGCGGGTTCTGGCGTTTGTGAT AATGG	
FGSG07925BR	ACTTGTATGTCCTCGTCGTCT	
FGSG07925OF	ATCACCGCTCGTGCTTTC	Verification of *ΔFgsg07925*
FGSG07925OR	TGTTGTCGCCGATAATGC	
FGSG07925UA	TTGTTGGAGGTGGTTGAGCC	
FGSG07925CF	agggaacaaaagctgggtaccTTGTTGGAGGTGGTTGAGCC	Complementation of *ΔFgsg07925*
FGSG07925CR	gcccttgctcaccataagcttCTCCTCAGATGGAGCGCCC	